A PARAMETRIC STUDY OF DRIFT STABILITY IN JOINTED ROCK MASS

PHASE II: DISCRETE ELEMENT DYNAMIC ANALYSIS OF UNBACKFILLED DRIFTS

Prepared for

Nuclear Regulatory Commission
Contract NRC-02-93-005

Prepared by

Center for Nuclear Waste Regulatory Analyses
San Antonio, Texas

June 1997

CNWRA 97-007

A PARAMETRIC STUDY OF DRIFT STABILITY IN JOINTED ROCK MASS

PHASE II: DISCRETE ELEMENT DYNAMIC ANALYSIS OF UNBACKFILLED DRIFTS

Prepared for

Nuclear Regulatory Commission
Contract NRC-02-93-005

Prepared by

Mikko P. Ahola

Center for Nuclear Waste Regulatory Analyses
San Antonio, Texas

June 1997

PREVIOUS REPORTS IN SERIES

Number	Name	Date Issued
CNWRA 96-009	A Parametric Study of Drift Stability in Jointed Rock Mass - Phase I: Discrete Element Thermal-Mechanical Analysis of Unbackfilled Drifts	September 1996
NUREG/CR-6388 CNWRA 95-013	Seismic Response of Rock Joints and Jointed Rock Mass	June 1996
CNWRA 95-012	An Experimental Scale-Model Study of Seismic Response of an Underground Opening in Jointed Rock Mass	June 1995
NUREG/CR-6021 CNWRA 92-001	A Literature Review of Coupled Thermal-Hydrologic-Mechanical-Chemical Processes Pertinent to the Proposed High-Level Nuclear Waste Repository at Yucca Mountain	July 1993
CNWRA 92-012	Field Site Investigation: Effect of Mine Seismicity on a Jointed Rock Mass	December 1992
NUREG/CR-5440 CNWRA 89-001	Critical Assessment of Seismic and Geomechanics Literature Related to a High-Level Nuclear Waste Repository	June 1991

ABSTRACT

Long-term stability of waste emplacement drifts is of interest in assessing the safety of disposal of high-level nuclear waste (HLW) in the proposed repository at Yucca Mountain (YM). As the repository preclosure operation period is envisioned to be about 100-150 yr, and the decision regarding the use of backfill in the emplacement drifts during the postclosure period of about 10,000 yr has not been finalized, the importance of long-term drift stability remains. Two significant factors that can induce drift instability include thermal loads generated by the decay of emplaced waste and repeated seismic loads from earthquakes. One of the failure mechanisms for an excavation in a jointed rock mass subjected to repeated seismic loading is through accumulation of shear displacements along joints. These dynamic ground motions, which are anticipated to occur at the YM site due to earthquakes (and possible nearby weapons testing), will subject repository emplacement drifts to dynamic stresses superimposed on excavation and thermal-induced stresses.

This report presents a discrete element analysis using the code UDEC (Version 3.0) to investigate the effect of repeated seismic loading, with peak underground accelerations ranging from 0.2 to 0.4g, on cumulative joint slip and failure around a heated and unsupported emplacement drift in the proposed repository at YM. A 100-MTU/acre thermal loading was used, as this is the upper bound of repository thermal loading considered by DOE (TRW Environmental Safety Systems Inc., 1997; CRWMS M&O, 1996). Analyses indicate that slip along joints and closure of the drift take place with both single and repeated episodes of earthquake loading to a larger degree if the rock mass around the drift is in a weakened or yielded state after the thermal loading and prior to the dynamic loading. If the rock remains in the elastic state after the thermal loading is applied, however, no measurable cumulative slip on joints or drift convergence is evident with repeated episodes of seismic loading up to 0.4g, aside from that which occurs during the first sequence of seismic loading. The maximum total roof deflection and joint shear displacement after two repeated episodes of earthquake loading were approximately 1.8 cm and 6.3 cm, respectively, for the range of dynamic loadings and cases considered.

CONTENTS

FIGURES

FIGURES (cont'd)

TABLES

ACKNOWLEDGMENTS

This report was prepared to document work performed by the Center for Nuclear Waste Regulatory Analyses (CNWRA) for the Nuclear Regulatory Commission (NRC) under Contract No. NRC-02-93-005. The activities reported here were performed on behalf of the NRC Office of Nuclear Material Safety and Safeguards, Division of Waste Management. The report is an independent product of the CNWRA and does not necessarily reflect the views or regulatory position of the NRC.

The author thanks Amit Ghosh and Wesley Patrick for their reviews of this report. The author is thankful to Yolanda Lozano for skillful typing of the report and to Corky Gray, who provided a full range of expert editorial services in the preparation of the final document.

QUALITY OF DATA

All CNWRA-generated data contained in this report meet quality assurance (QA) requirements described in the CNWRA Quality Assurance Manual. Sources for other data should be consulted for determining the level of quality for those data. Several utility software packages developed at the CNWRA were used for analyses of data contained in this report. These software packages fall under the categories covered by QAP-014, Documentation and Verification of Routine Calculations, and are not controlled by configuration management procedure TOP-018.

SOFTWARE QUALITY ASSURANCE

The distinct element code UDEC (Version 3.0), used for all the dynamic runs, is controlled under the CNWRA software QA procedure (TOP-018, Development and Control of Scientific and Engineering Software).

EXECUTIVE SUMMARY

Emplacement of heat generating radioactive waste in the partially saturated and fractured geologic medium of Yucca Mountain (YM) will induce thermal, mechanical, hydrological, and chemical processes, some of which may have significant effects either directly or through couplings among the processes. It is assumed that mechanical processes include dynamic phenomena such as earthquake loading. A Nuclear Regulatory Commission (NRC) staff technical position (Nataraja and Brandshaug, 1992) provided an acceptable methodology for systematically considering thermal loads and thermally induced mechanical, hydrological, and chemical processes for the design and performance assessment (PA) of a proposed geologic repository. This staff technical position is applicable to the U.S. Department of Energy (DOE) demonstration of compliance with NRC regulations on thermal loads (Nuclear Regulatory Commission, 1996). When processes are coupled, behavior of the repository and surrounding rock mass cannot be reasonably evaluated by considering each process independently (Wang et al., 1983; Tsang, 1987; Manteufel et al., 1993). The importance of various processes and their couplings will depend upon the thermal loading of the repository, the design of the engineered barriers including backfills, the properties of the geologic medium, the time and spatial scales at which these processes are of interest, and the measures selected to evaluate performance.

A key technical issue (KTI) in the high-level nuclear waste (HLW) program is evaluation of time-dependent thermal-mechanical (TM) coupled response of the jointed rock mass. Postclosure PA requires an understanding of the TM response of a jointed rock mass over the compliance period (thousands of years) as it impacts the near-field environment and waste package degradation, performance of seals, and flow and radionuclide transport mechanisms. Design for the preclosure operation period ($\approx$ 100–150 yr) requires an understanding of the TM response of the jointed rock mass as it influences drift stability and waste retrievability. Two activities that involve study of mechanical effects in the near-field environment of the proposed HLW repository are (i) stability of underground excavations, including emplacement drifts, for both opening design and providing input for design and PA of waste packages; and (ii) change of hydrological properties of rock fractures due to TM perturbation of the rock mass.

A TM parametric study is being conducted in a phased approach to identify thermal as well as site-specific static and dynamic loadings, and rock mechanical and thermal parameters that may significantly influence the pre- and postclosure performance of the repository under heated and seismic conditions. The Phase I study (Ahola et al., 1996) was completed earlier and consisted of a discrete element parametric study of emplacement drifts without backfill, rock support, or seismic load for 100 yr of heating using UDEC. The work presented herein is the Phase II study, a continuation of the Phase I study to include the dynamic loading; however, it was much more limited in scope than the Phase I study due to programmatic constraints for this particular KTI.

Previous research activities conducted by the Center for Nuclear Waste Regulatory Analyses (CNWRA), including a literature review (Kana et al., 1991) as well as both laboratory-scale and field-scale experiments (Kana et al., 1995; and Hsiung et al., 1992a and b), revealed that repeated ground motions due to seismic activity may influence both the short- and long-term performance of a repository. With regard to waste retrievability and/or mechanical integrity of the waste package itself, this impact may come from emplacement drift instability as a result of accumulated shear displacements along joints intersecting the drift. The literature on earthquake effects on underground structures generally addresses only the effects of a single earthquake event, because of the shorter required life span of such structures

and the time gap between events. Field observations have generally demonstrated that underground openings are more stable than surface structures during a strong earthquake (Lee et al., 1982). Dowding and Rozen (1978) studied the response of 71 drifts to strong ground motion in California, Alaska, and Japan. The results indicated that, at peak accelerations that caused heavy damage to surface structures, there was only minor damage to the tunnels. Dowding (1985) showed from case studies, based on estimated peak particle velocities (v_s) at the ground surface, that earthquake damage to tunnels could be classified into three categories: (i) no damage ($v_s < 20$ cm/s), (ii) minor damage ($20 < v_s < 90$ cm/s), and (iii) damage ($v_s > 90$ cm/s). For this particular study, based on earthquake hazard curves for YM and utilizing a ground motion reduction factor of 0.5 for the subsurface, the range of peak underground velocities simulated were between 20-40 cm/s (i.e., 40–80 cm/s at ground surface). Thus, under these earthquake loading conditions, a typical underground tunnel would be expected to incur minor damage, at worst, from single earthquake events.

In a repository environment, however, underground waste emplacement drifts are required to maintain their stability over a much longer time frame and be subjected to high TM induced stresses. Such long time frames will result in more deterioration of the rock around the drifts, as well as the possibility of yielding and increased fracturing of the near-field rock during the thermal loading period. Also, such waste emplacement drifts would be expected to encounter multiple episodes of seismic loading. As a result, the overall objective of this Phase II study was to perform a limited amount of numerical modeling to estimate the significance of repeated seismic loading on heated, underground waste emplacement drifts. It should be mentioned that all dynamic loadings were applied near the time of maximum thermal loading (≈ 100 yr) including repeated dynamic loadings. A thermal load of 100 MTU/acre was chosen for the dynamic analyses. From the Phase I study, this thermal load was found to have the most adverse effect on the preclosure repository drift performance. Also, based on the DOE repository advanced conceptual design, the 100 MTU/acre thermal loading is considered as an upper bound (TRW Environmental Safety Systems Inc., 1994; CRWMS M&O, 1996). Due to difficulties in running the thermal analysis out to long time periods (i.e., thousands of years) it was not possible to address the effect of seismic loadings during the cool down period.

Two cases from the Phase I TM study were chosen for this dynamic study (Phase II), one being the worst scenario case from the TM analysis in terms of the amount of rock mass yielding, the other being a possible scenario where no yielding of the intact rock occurred during thermal loading. The Phase II study considered earthquake loadings ranging from 0.2 to 0.4g peak underground accelerations, and both single and repeated events were considered. Cumulative joint shear displacement and/or drift convergence were experienced to some degree with repeated seismic loading for all cases analyzed, however, to a much greater degree for the worst case scenario chosen from the Phase I TM study. The maximum total roof deflection and maximum joint shear displacement were 1.8 cm and 6.3 cm, respectively, for all cases and dynamic loading conditions considered. Although some rock became unstable during the TM loading stage, no additional instability (in terms of rockfall) was evident during the dynamic loading stage. Additional rock mass yielding was observed, however, during some of the dynamic runs indicating the possibility for localized rock failure around the drift. A steeper orientation vertical joint set (as measured from the horizontal) resulted in the rock mass being more sensitive to the TM as well as dynamic loading stages in terms of the extent of the yield zone, maximum joint shear displacements, and drift closure.

Various assumptions and limitations were necessary in the Phase II dynamic drift stability analysis. For example, for computational purposes, only the wider joint spacings from the Phase I study could be considered for the Phase II dynamic study, which may not be truly representative of the underground repository environment. Consequently the modeling results should be compared with field measurement

and/or field-scale test results, where applicable, to gain further confidence in the results from the dynamic stability analyses. No data are presently available to calibrate the model against drift convergence measurements during excavation or similar field-scale test results for rock deformations due to heating, prior to this dynamic stability study. However, DOE will be conducting field tests (e.g., single heater test, drift-scale heater test) that would support such comparisons.

1 INTRODUCTION

1.1 BACKGROUND AND OBJECTIVES

Yucca Mountain (YM), in southern Nevada, has been designated by the United States Congress for characterization as a potential repository site for high-level nuclear waste (HLW) disposal. A general description of the YM site for the proposed HLW repository was presented in the U.S. Department of Energy (DOE) Site Characterization Plan (SCP) (U.S. Department of Energy, 1988). In addition, progress on YM site characterization, design, and testing is documented by the DOE through its semiannual SCP reports.

The YM area is characterized by north to northwest-trending mountain ranges composed of volcanic strata that dip eastward. The strata are broken into en-echelon fault blocks. The geomechanical conditions at the site are characterized by a highly fractured rock mass with prominent vertical and sub-vertical faults and joints that transect the site environs. Arid climate prevails in the YM area, with less than 25 cm of rain per year, and no perennial streams exist in this region. The potential repository location is in the densely welded, devitrified part of the Topopah Spring (TSw2 unit) member of the Paintbrush tuff, which is about 350 m below the ground surface and 225 m above the water table (Klavetter and Peters, 1986; CRWMS M&O, 1994a). The emplacement of radioactive waste in this partially saturated geologic medium will induce thermal, mechanical, hydrological, and chemical processes, some of which may have significant effects either directly or through couplings among the processes. When processes are coupled, behavior of the repository and its surrounding rock mass cannot be reasonably evaluated by considering each process independently (Wang et al., 1983; Tsang, 1987; Manteufel et al., 1993). The importance of various processes and their couplings will depend on the thermal loading of the repository, the design of the engineered barriers including backfill, the properties of the geologic medium, the time and spatial scales at which these processes are of interest, and the measures selected to evaluate performance.

The fractured rock mass will be perturbed in several ways. First, construction of the repository alters the state of stress which, in turn, causes mechanical deformation of the rock, including joint normal and shear deformations. Joint normal and shear deformations affect excavation stability. They also affect fluid flow and solute transport in the rock mass, which are particularly important to the performance of a HLW geologic repository and its environment. Second, nuclear waste provides a heat source that is active over an extended period of time. This thermal load induces rock expansion, which may cause dilation, closure, and shear failure of fractures. Furthermore, the thermal load could also induce microfracturing of intact rock due to thermal expansion as well as possible buildup of pore pressure due to vaporization of the water. As a result, permeability of both matrix and fracture may change accordingly. The thermal load may also cause (i) degradation of the mechanical properties of the rock mass (Price et al., 1987); (ii) changes to the chemical sorption and retardation capabilities; (iii) vaporization, vapor flow, condensation, and condensate flow (Manteufel et al., 1993); and (iv) dissolution of rock matrix or fracture fillings, or healing or rock fractures through mineral precipitation (Lin and Daily, 1989; de Marsily, 1987). Third, dynamic ground motions from earthquakes and nearby underground nuclear weapons testing will induce additional stresses. The dynamic ground motions, including the cumulative effect of repeated seismic motions, will cause further dilation, closure, and shear of fractures, which may change fracture permeabilities (Kana et al., 1991 and 1995).

A recent Nuclear Regulatory Commission (NRC) staff technical position provided an acceptable methodology for systematically considering thermal loads and thermally induced mechanical, hydrological, and chemical processes in design (Nataraja and Brandshaug, 1992). The primary purpose of the NRC technical position is to outline an acceptable method of comprehensively, systematically, and logically understanding and evaluating coupled process response for design and performance assessment (PA) of a proposed geologic repository. This staff technical position is applicable to the DOE demonstration of compliance with NRC regulations on thermal loads (Nuclear Regulatory Commission, 1996).

A key technical issue (KTI) identified by the NRC in the HLW program is evaluation of thermal-mechanical (TM) coupled response of the jointed rock mass. Postclosure PA requires an understanding of the TM response of the jointed rock mass over the compliance period (thousands of years) as it affects near-field environment and waste package (WP) degradation, performance of seals, and flow and radionuclide transport mechanisms. Also, designing for the preclosure or operations period ($\approx$100–150 yr) requires an understanding the TM response of the jointed rock mass as it influences drift stability and retrievability.

In general, there are two factors that involve mechanical effects in the near-field environment of the proposed HLW repository: (i) stability of underground excavations, including emplacement drifts and (ii) change of hydrological properties of rock fractures due to TM perturbation of the repository rock. The first factor is important to opening design and PA of WPs, while the second factor is essential to WP and total system performance.

Stability of underground openings, including emplacement drifts, will primarily depend on TM effects. The TM effects are those resulting from excavation-induced stresses, dynamic motions, including the cumulative effect of repeated seismic motions, and thermally induced stresses and deformations (Ghosh et al., 1994). Movement along joints in the disturbed rock mass forms the primary mode of deformation of the near-field rock mass (Kana et al., 1991, 1995; Hsiung et al., 1992a and 1992b). Excessive slippage of a rock block along failed joints may affect performance of the waste canisters inside emplacement drifts. In addition to the TM effects, behavior of the joints is also influenced by the presence of water (Jaeger and Cook, 1979; Hoek and Brown, 1980), changes in temperature, and time-dependent degradation of mechanical properties of rock matrix and joints (Kemeny and Cook, 1990; Price et al., 1987).

It is well recognized that rock strength and joint properties are functions of time, stress, and temperature; that is, rock mass deteriorates as time passes and/or temperature increases (Martin, 1972; Nimick and Connolly, 1991; Price et al., 1987; Carter, 1975, 1976). Time-dependent decrease in shear strength of joints may be due to (i) fracture wall-rock alteration as a result of extended exposure to heat and moisture, (ii) slow deformation of asperities as a result of sustained stress concentration, and (iii) possible increase in fracture wall-rock ductility as a result of exposure to heat. The time-dependent decrease in strength of intact rock is generally associated with (i) gradual slip on grain contacts under sustained stress concentration, (ii) subcritical crack growth due to sustained stress concentration and chemical effects at microcrack tips, and (iii) possible increase in ductility (decrease in viscosity) of minerals due to exposure to heat (Althaus et al., 1994).

Backfill could be placed in the emplacement drifts by the DOE (TRW Environmental Safety Systems, Inc., 1994) for three major reasons: (i) to minimize deleterious rock movement in the strata between the surface and the repository horizon that may cause surface subsidence; (ii) to protect or

cushion the WP from rock falls; and (iii) to retard transport of radionuclides to the accessible environment. Stability of emplacement drifts and the thermal environment in these drifts will be significantly affected by the absence or presence of backfill in the emplacement drifts. Consequently, TM effects on WPs will also be significantly influenced by backfill.

The TM response of a jointed rock mass is affected by a number of parameters and conditions: (i) rock properties such as Young's modulus, strengths (tensile, compressive, and shear), Poisson's ratio, density, cohesion, specific heat, friction angle, coefficient of thermal expansion and thermal conductivity, and their variations with temperature, time, moisture content, and space; (ii) joint properties such as normal and shear stiffnesses, cohesion, angle of friction, tensile strength, orientation and spacing of joints, and their variations with temperature, time, moisture content, and space; and (iii) *in situ* stresses, construction of openings, single and multiple seismic events, thermal loads, and their variations with time. Parametric analysis involving these parameters and conditions provides an effective means to identify important influences on coupled TM response of a jointed rock mass for both opening stability and fracture permeability change.

The overall objective of the TM parametric study is to identify thermal as well as static and dynamic loadings, and rock mechanical and thermal properties that may significantly influence the pre- and postclosure performance of the repository under heated and seismic conditions. A phased approach was adopted for this purpose.

The activities associated with the Phase I TM parametric study were completed and reported in 1996 (Ahola et al., 1996). The objective of the Phase I study was to conduct a parametric investigation of emplacement drifts without backfill, rock support, and seismic load for 100 yr of heating using the distinct element code UDEC (Version 2.01). In the Phase I study, a 2^k fractional factorial experimental design approach was adopted. The 2^k fractional factorial design studies the effect on system response of k parameters, each at two levels. Nine parameters (k=9) were studied: subvertical and subhorizontal joint inclination [measured counterclockwise from the horizontal axis assuming strike of joints that are parallel to the drift axis], subvertical joint spacing, joint friction angle, thermal load, intact rock cohesion, intact rock friction angle, intact rock Young's modulus, and thermal expansion coefficient. The two levels were low and high values of these parameters. Although a full 2^9 factorial plan would require 512 runs, in the Phase I analysis only 64 runs (i.e., 1/8 fractional factorial plan) were made. The performance measures used in that study included: maximum and minimum principal stresses around the excavation, maximum joint shear displacement, maximum joint closure, maximum joint separation, roof-to-floor convergence, and extent of yield zone around the excavation.

The objective of this Phase II study is to analyze the mechanical response of an unbackfilled, unsupported emplacement drift subjected to combined excavation and thermally induced stresses, and seismic induced stresses. In particular, the affect of repeated seismic landings on emplacement drift stability is addressed, as it has long been thought that jointed rock may be more susceptible to fatigue damage and ultimate collapse than intact rock (Brown and Hudson, 1974), and that there might be some threshold value of seismic input amplitude required before any significant amount of permanent rock mass deformation will occur and begin to accumulate (Kana et al., 1995). The scope of the Phase II study was scaled down considerably due to programmatic constraints that required rapid close-out and wrap-up of the TM related KTI. Two separate cases involving different joint and intact rock properties and strength parameters were analyzed. These two cases were selected from the Phase I study (Ahola et al., 1996). Of the two cases selected, one was most sensitive to the effects of TM loading in that a large zone of rock mass yielding developed around the emplacement drift. The other case contained a set of rock and joint

properties and strength parameters in which no rock mass yielding occurred as a result of thermal loading. For each case, two levels of seismic loading were applied to the model. Furthermore, for each level of seismic loading, the seismic load was repeated twice. For simplicity, the second cycle was applied almost immediately after the first, which was applied at the end of the TM analysis period [100 yr after emplacement of the canisters (i.e., near the end of the proposed pre-closure period)]. A more representative approach would have been to apply the earthquake loadings at different periods of time depending on their likely probability of occurrence. For instance, the first earthquake loading could be applied at $t = 100$ yr near the peak thermal-load, and the second one sometime later during the cool down period. This was not practical for the present UDEC (Version 3.0) analysis since a rather small thermal time step was required during the TM analysis. This was because the thermal logic scheme within UDEC utilizes a continuum model, and does not appear to converge easily with large mechanical slip and/or separation among discrete blocks, especially in the unsupported, heated-drift scenario. Even increasing various tolerances, it was not possible to increase the thermal time step to a great extent.

1.2 SCOPE

The reduced scope of Phase II of the multiphase parametric study reported here includes

- selecting two cases from the TM parametric study conducted under Phase I
- rerunning the TM analysis with the lateral model dimensions extended to include three emplacement drifts (it was judged to be necessary to extend the lateral boundaries for the dynamic shear wave study)
- simulating a range of peak earthquake ground motions (0.2g to 0.4g peak ground accelerations), including repeated events

2 PARAMETERS AND MODEL GEOMETRY

2.1 MECHANICAL AND THERMAL PROPERTY DATA INPUT

As mentioned in the introduction, the entire TM and dynamic analysis was conducted for two different sets of intact rock and joint properties, identified as Cases A and B and shown in table 2-1. One set of mechanical and thermal properties (Case A) resulted in no rock mass yielding after 100 yr of thermal loading, assuming a Mohr-Coulomb plasticity model for the intact rock. The other set of mechanical and thermal properties (Case B), however, resulted in a large zone of yielding within the rock mass after 100 yr of thermal loading and prior to the dynamic loading. Thus, Case B could be considered to already be in a damaged or weakened state prior to the dynamic loading. As shown in table 2-1, aside from Young's modulus, the primary difference between Cases A and B was in the strength properties of both the intact rock and rock joints. The joint patterns were the same in both cases. However, to obtain some idea of the effect of joint orientation (particularly the subvertical joints) on the dynamic response of the drift, Case B was modified to include a subvertical joint orientation of 70° versus 85° as shown in table 2-1. This modified case will be referred to as Case B1 in the discussion of the results in section 4. DOE site characterization shows that the moderately to densely welded, thermal/mechanical TSw2 unit consists of intact blocks separated by planar fractures. Results of mapping in the access drift (Barr et al., 1996) indicate that the fracture system consists of two sets of predominantly vertical fractures (the most dominant of which has a roughly NW strike and the second with a NE strike), and a low-angle set with a NW strike. The joint orientations shown in table 2-1 along with the modified Case B, were intended to encompass the range of fracture data measured in the field, taking into consideration that the analysis is only 2D and that only a selected few dynamic runs could be made.

Regarding joint spacings, the repository rock is more fractured than the overlying units, with an overall fracture density of about 4 fractures/m (i.e., 0.25 m spacing) in the ESF tunnel interval from station 27+00 to 56+30 and local average densities in any 400- to 500-m segment ranging from about two to six fractures/m (Wilder, 1996). Although the Phase I TM parametric study considered subvertical joint spacings down to a density of 4 fractures/m (0.25 m spacing), the Phase II dynamic study (for computational purposes) only treated fracture densities of 2 fractures/m (0.5 m spacing) as indicated in table 2-1. The fact that the dynamic study utilizes a somewhat lower fracture density than measured in the field should be taken into account in interpreting the results of the Phase II dynamic drift stability study.

2.2 SEISMIC INPUT

The earthquake input used in the analysis was taken from ground motion records from an earthquake that took place in Mexico City on September 19, 1985. The duration of this earthquake was approximately 30 s with a predominant frequency of 0.5 Hz, typical of most earthquakes. Some baseline correction was necessary for the velocity record (input to the UDEC analyses) to assure that, as the velocity approached zero at the end of the earthquake duration, the integrated displacement also approached zero. Only some minor adjustments to the velocity record were necessary in order to accomplish this. For this analysis, three different levels of earthquake loadings were applied to the model. These three loadings corresponded to peak underground accelerations of 0.2g, 0.3g, and 0.4g, which were generated by scaling the amplitude of the actual earthquake signal accordingly. Since the model domain used actual dimensions, it was decided that scaling time would not be appropriate. Thus, the full 30-s earthquake history was applied with scaling applied only to the amplitude to develop the desired

Table 2-1. Input rock and joint parameters for the dynamic study

Parameters	Case A	Case B
Young's Modulus (GPa)	16.0	32.0
Poisson's Ratio	0.21	0.21
Rock Friction Angle (deg)	50.0	20.0
Rock Cohesion (MPa)	18.0	18.0
Thermal Expansion Coeff. (K^{-1})	12.0×10^{-6}	12.0×10^{-6}
Near-field Subvertical Joint Orientation (deg)	85.0	85.0
Near-field Subhorizontal Joint Orientation (deg)	10.0	10.0
Near-field Subvertical Joint Spacing (m)	0.5	0.5
Near-field Subhorizontal Joint Spacing (m)	1.0	1.0
Joint Friction Angle (deg)	38.0	28.0
Joint Cohesion (MPa)	0.08	0.08
Joint Tensile Strength (MPa)	0.04	0.04
Rock Tensile Strength (MPa)	5.0	5.0
Rock Density (kg/m^3)	2297.0	2297.0
Joint Normal and Shear Stiffnesses (MPa/m)	1.0×0^5	1.0×10^5
Thermal Conductivity (W/m-K)	2.1	2.1
Specific Heat (J/kg-K)	932.0	932.0

input motion. Figure 2-1 shows the input earthquake velocity and displacement profiles corresponding to a 0.4g peak surface acceleration.

The input seismic motion was converted to either a shear or compressive stress wave and applied to the base of the model. The conversion from a velocity input as shown in figure 2-1 to a stress input can be made utilizing the following equations (Itasca Consulting Group, Inc., 1996)

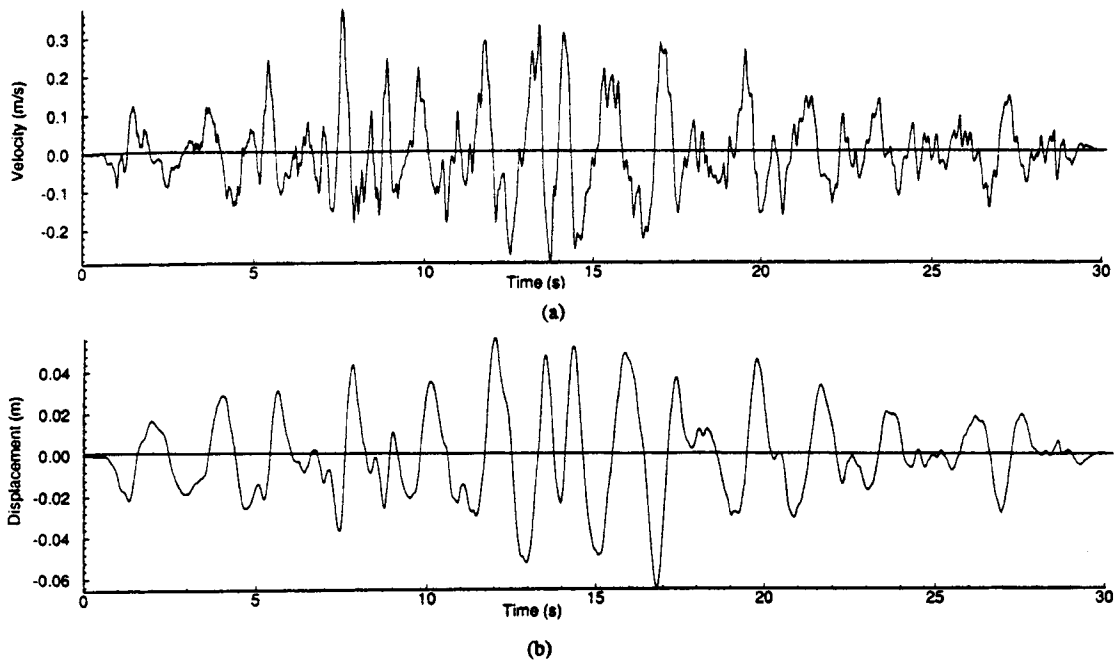

Figure 2-1. Input seismic motion records for (a) velocity, and (b) displacement

$$\sigma_n = 2(\rho C_p)v_n \tag{2-1}$$

$$\sigma_s = 2(\rho C_s)v_s \tag{2-2}$$

where
- σ_n = applied normal stress,
- σ_s = applied shear stress,
- ρ = mass density,
- C_p = speed of p-wave propagation through medium,
- C_s = speed of s-wave propagation through medium,
- v_n = input normal particle velocity, and
- v_s = input shear particle velocity.

C_p is given by

$$C_p = \sqrt{\frac{K + 4G/3}{\rho}} \tag{2-3}$$

and C_s is given by

$$C_s = \sqrt{G/\rho} \tag{2-4}$$

where K and G are bulk and shear moduli, respectively. The above equations assume plane-wave conditions. The factor of two in Eq. (2-1) and (2-2) accounts for the fact that the applied stress must be doubled to overcome the effect of the viscous bottom boundary (as discussed later in section 2-4).

The effect of repeated seismic motion was investigated by applying a second signal of the same magnitude to the base of the model, delayed 5 s from the first, to see if cumulative damage occurred. Typical seismic hazard curves for YM as shown in figure 2-2 (Hoffman, 1994) are based on surface earthquake motion. For instance, based on figure 2-2, an earthquake having a ground acceleration of 400 mm/s^2 (i.e., 0.4g) would have a likely return period of approximately 1,400 yr, using the 50 percentile curve. Thus, based on statistics, one would assume that such an earthquake would take place more than once during a 10,000 yr repository postclosure performance period. At the repository depth of 300 m, the ground motion is significantly reduced. DOE published ground motion reduction factors of the ESF design (table 2-2) shows that, at the 300-m repository depth, one can expect reduction factors to be 0.5 and 0.6 for the horizontal and vertical peak accelerations, respectively (CRWMS M&O, 1994b; Department of Energy, 1995). Thus, a 0.4g ground acceleration at the ground surface (from figure 2-2) would correspond to approximately a 0.2g peak acceleration at the repository depth. Thus, based on the seismic hazard curves for YM, an earthquake having a peak underground acceleration of 0.2g (0.4g at ground surface) would be expected to occur more than once during the repository postclosure performance period. The possibilities of repeated earthquakes having peak underground accelerations of 0.3g and 0.4g (0.6g and 0.8g, respectively, at ground surface) are more remote depending on which constant percentile curve is chosen, and their consideration in this Phase II study represents a conservative assumption.

Table 2-2. Ground motion reduction factors as a function of depth for ESF design (CRWMS M&O, 1994b)

	Peak Velocity		Peak Acceleration	
Depth (m)	**Horizontal**	**Vertical**	**Horizontal**	**Vertical**
0-100	1.00	1.00	1.00	1.00
100-200	0.70	0.80	0.60	0.70
200-400	0.60	0.70	0.50	0.60
>400	0.55	0.60	0.50	0.50

2.3 THERMAL-MECHANICAL ANALYSES MODEL

As stated earlier, the intent of the analyses was to investigate the effect of repeated seismic loading on an emplacement drift under excavation-induced and thermally induced stresses. To achieve this objective, the analyses first considered a large domain for conducting the TM analysis, followed by utilizing a smaller subdomain around the immediate tunnel for the dynamic analysis. The domain for the

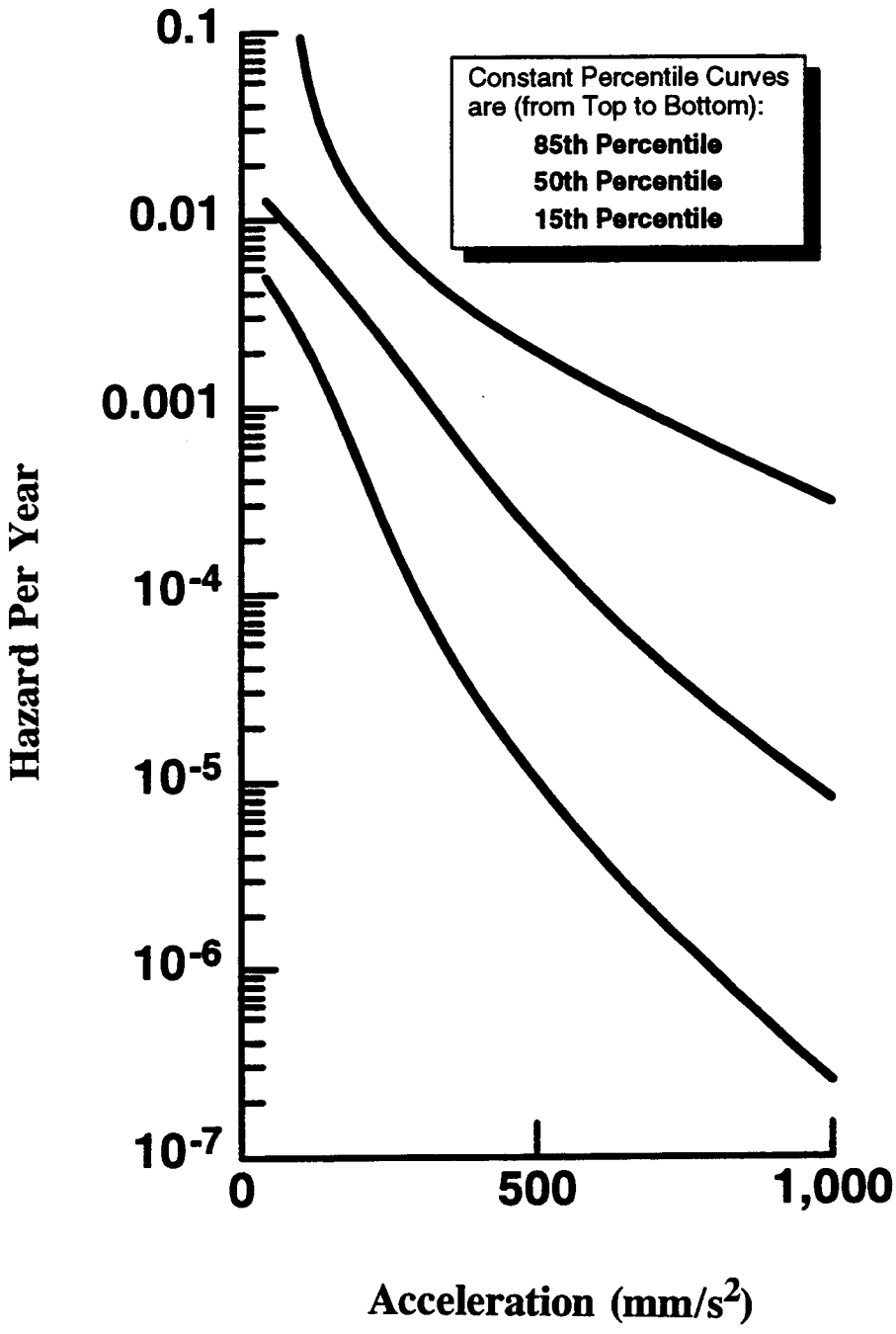

Figure 2-2. Seismic hazard curves based on faulting at Yucca Mountain (Hoffman, 1994)

TM analysis extended 300 m above the waste emplacement horizon (i.e., up to the mean ground surface) to 300 m below, so as to not artificially affect the propagation of heat. However, unlike the Phase I TM analyses in which the models incorporated only one drift, the Phase II dynamic analyses models included three drifts. It was judged necessary to extend the lateral boundaries outward for the dynamic motion. Detailed jointing, however, was included only around the central drift, in order to limit the size of the model in terms of the number of discrete blocks and finite difference zones within the deformable blocks. Figure 2-3 shows the large-scale model comprised of discrete element blocks.

For the TM analysis, the two vertical boundaries are rollered with a thermal boundary condition of zero heat flux. The top boundary representing the ground surface was stress free allowing for upward thermal expansion, while the bottom boundary was fixed in the vertical direction. Temperature boundary conditions were applied at the top and base of the model, as well as initially throughout based on a uniform geothermal gradient of 0.02 °C/m. The *in situ* mechanical stress state at the repository horizon was set to a 7.0 MPa vertical stress and 3.5 MPa horizontal stress, based on average measured values in DOE's advanced conceptual design (CRWMS M&O, 1996). The vertical stress gradient with depth, based on a uniform rock density of 2,580 kg/m^3, was input as 0.0233 MPa/m. The horizontal stress gradient with depth was taken to be one-half the vertical stress gradient. The stress gradients were calculated such that the vertical and horizontal stresses were equal to zero at the ground surface and equal to 7.0 and 3.5 MPa, respectively, at the 300 M repository emplacement horizon. After excavation, the thermal load applied to the rock mass prior to the dynamic study was 100 MTU/acre (2.471×10^{-2} metric tons of uranium/m^2), and it was accomplished by applying a heat flux directly to the emplacement drift

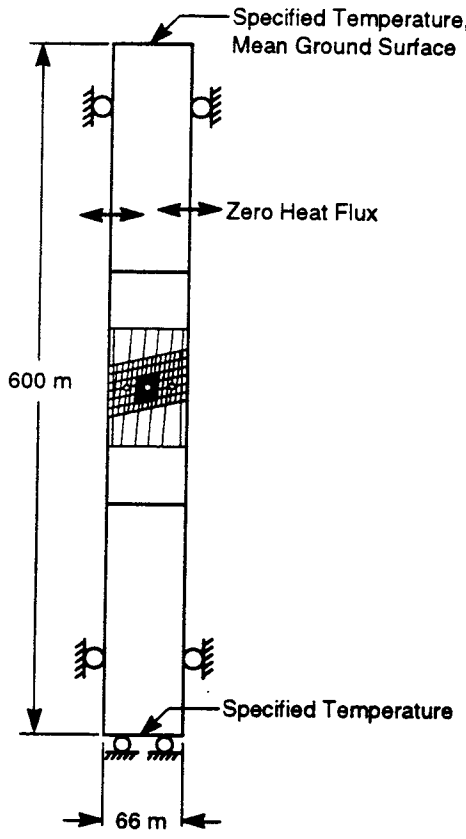

Figure 2-3. Large-scale discrete element model for thermal-mechanical analysis

wall for all three drifts, since UDEC does not simulate cavity radiation. This 100 MTU/acre thermal loading is the upper bound considered in DOE's advanced conceptual design (CRWMS M&O, 1996), and it was also found to have the most impact on preclosure repository drift performance from the Phase I study. For this 100 MTU/acre thermal loading, a drift spacing of 22 m was used. The TM loading was run to a time state of 100 yr. The remainder of the TM solution process is described in more detail by Ahola et al. (1996).

2.4 DYNAMIC ANALYSES MODEL

Upon completion of the thermal loading stage, it was decided to utilize a smaller subdomain of the original problem domain for the dynamic analysis. This was done to simplify the problem, reduce the number of discrete element blocks and finite difference zones and, thus, speed up the dynamic analysis, which has rather severe time step limitations. The final domain for the dynamic analysis extended 50 m above and below the repository horizon (figure 2-4). The dynamic run times placed limits on the joint spacings that could be accommodated around the central drift. For all cases, the minimum sub-vertical and sub-horizontal joint spacings around the central drift were 0.5 and 1.0 m, even though the Phase I study considered sub-vertical joint spacing as small as 0.25 m, which is more representative of joint mappings within the TSw2 unit. The types of dynamic boundary conditions varied depending on whether the dynamic wave was shear or compressive. Both types were investigated. Since the shear waves are generally more damaging and better represent the likely scenario, the majority of the dynamic runs

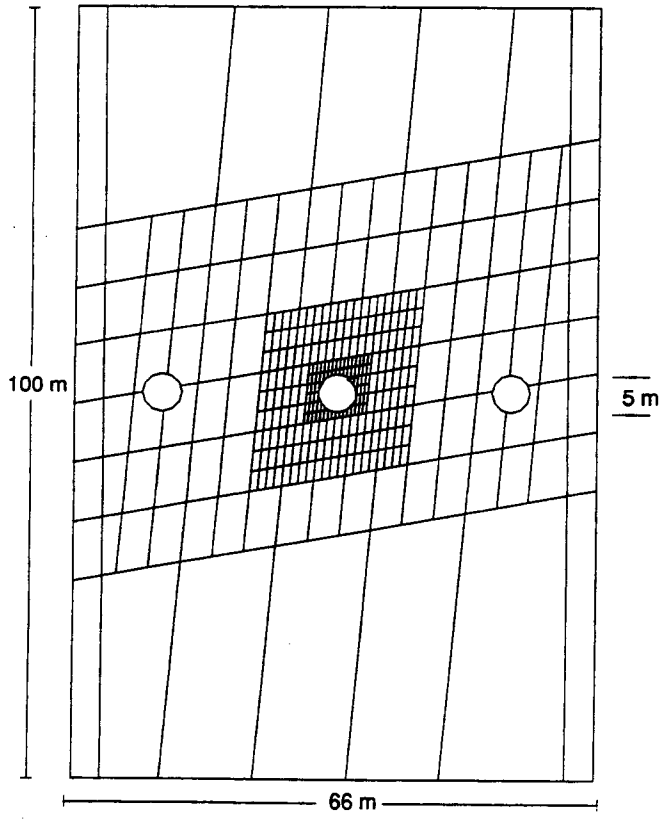

Figure 2-4. Sub-domain model for dynamic analysis

incorporated shear wave motion. For the vertically propagating compression wave, the vertical boundaries remained rollered, as was the case for the TM analysis. However, due to a limited vertical dimension, viscous non-reflecting boundary conditions were applied to the top and base of the dynamic model, after first solving for the new boundary stresses to be applied to these two boundaries of the submodel upon deleting the upper and lower portions from the large TM model. For the base of the model, this required inputting the earthquake signal as a stress wave rather than as a velocity time history since two velocity boundary conditions (i.e., viscous damping and earthquake velocity time history) cannot be applied at same boundary. As a result, reflections from the drifts would pass through the base. Although, in reality, some amount of reflection of dynamic waves from the ground surface occurs, the earlier dynamic models incorporating a full rock column including the ground surface, appeared to overpredict the magnitude of the reflected waves. This is due to the elastic behavior assumed and the inability to account for soil damping, etc. As a result, it was necessary to employ a viscous non-reflecting boundary on the top of the model. Figure 2-5 shows a schematic of the dynamic model (excluding the joints) along with boundary conditions for simulating the compression (P-wave) dynamic motion.

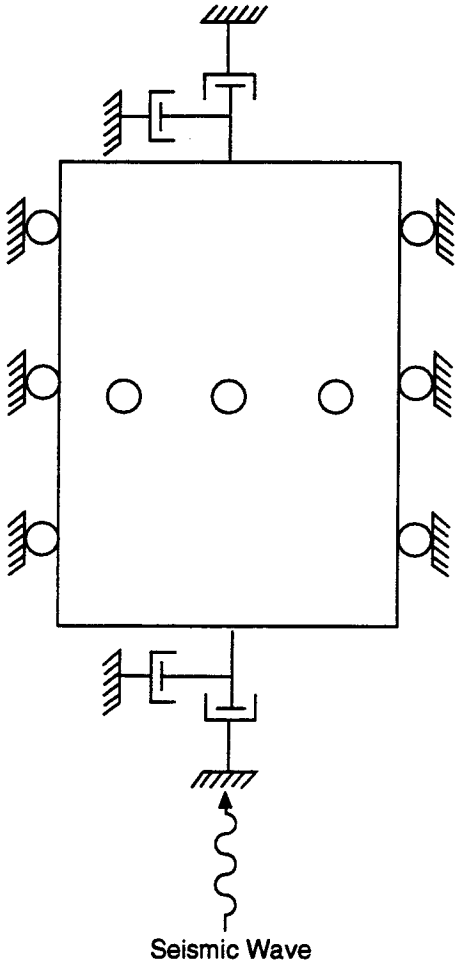

Figure 2-5. Schematic diagram showing boundary conditions for dynamic analysis of vertically propagating compression wave (joints not plotted)

Additional modifications to the dynamic model were necessary for simulating the propagation of shear wave (S-wave) ground motion. Namely, the rollers along the two vertical boundaries had to be removed and replaced with free-field boundaries to allow vertical propagation of the shear wave (Itasca Consulting Group, Inc. 1996). These free-field boundaries consist of one-dimensional columns of gridpoints under the *in situ* stress loading conditions, which are linked to the main model. Figure 2-6 shows a schematic of the dynamic model with the free-field boundaries for the dynamic shear wave analyses, excluding the joints for simplicity. Viscous non-reflecting boundary conditions are applied to the top and base of the one-dimensional free-field column, in addition to the dynamic shear wave applied to the base of the free-field columns. Removing the lateral roller boundary conditions and replacing them with free-field boundary conditions allows for accurate propagation of the vertical shear wave, while at the same time maintaining the TM stress state within the model.

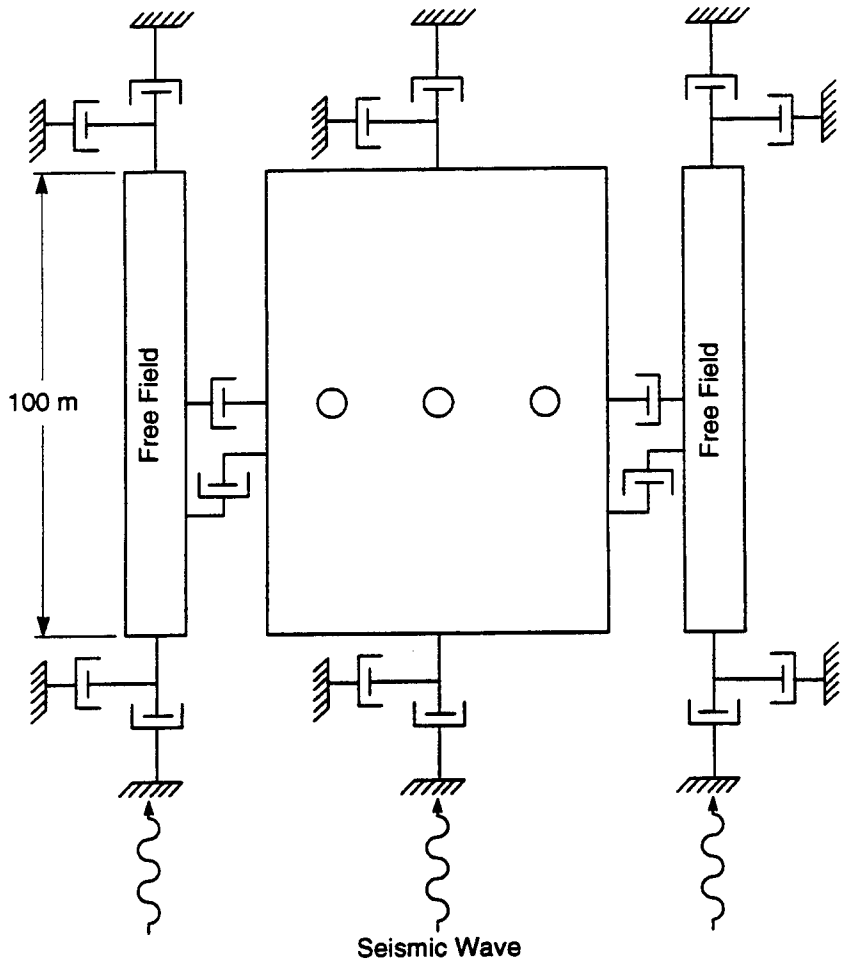

Figure 2-6. Schematic diagram showing boundary conditions for dynamic analysis of vertically propagating shear wave (joints not plotted)

3 MODELING APPROACH

3.1 MATRIX OF RUNS

Peak underground accelerations associated with the simulated earthquakes ranged from 0.2 to 0.4g. As a result of the long run times for the dynamic analysis, as elaborated on in the next section, only a select few runs were conducted to try to establish the range of dynamic responses an emplacement drift might experience. A small matrix of runs is presented in table 3-1, where each entry represents two repeated earthquake motions at the same magnitude. Only one run in the table incorporated compressive wave motion. All the dynamic runs for the heated drift scenario assumed, as initial conditions, a 100-yr TM loading state around the drift for both repeated dynamic motions. In addition, two dynamic runs were made assuming the drift was not heated (excavation-induced loading only), primarily for comparison.

3.2 DAMPING AND DYNAMIC TIME STEP

A small amount of damping (less than one percent) was applied at the dominant earthquake frequency that, based on the analysis of the frequency content of the input motion (i.e., figure 2-1), was found to be approximately 1 Hz. Slip along joints and material yielding already act as natural damping within the system. Both mass and stiffness-proportional damping (i.e., full Raleigh damping) were used in the analysis. However, a rather severe penalty on time step results when using stiffness-proportional damping, since the time step must be further reduced for numerical stability. If stiffness-proportional damping is not used, some very large accelerations are generated around the tunnel as a result of no damping applied to the high frequencies, since mass damping is inversely proportional to the frequency.

For this particular discrete element mesh, the stable dynamic time step required was on the order of 10^{-7} s, incorporating both mass and stiffness damping. Because of the long earthquake signal,

Table 3-1. Matrix of runs for UDEC Phase II dynamic analysis

	Peak Underground Acceleration	Case No.		
		Case A	Case B	Case B1
Excavation Stage	0.4g	—	Shear Wave	Shear Wave
Thermal Loading Stage (100 yr)	0.2g	Shear Wave	Shear Wave	—
	0.3g	—	Shear Wave Compression Wave	Shear Wave
	0.4g	Shear Wave	Shear Wave	—

it was necessary to apply some amount of partial density scaling to the blocks with small masses to increase the time step for computational purposes. In order to increase the time step up to the order of 10^{-5} s, approximately 290 gridpoints required density scaling out of a total of 2,200 gridpoints. At that time step, simulation of two consecutive 30-s earthquake loadings resulted in run times of approximately 12 days on a Sun Sparc 10 workstation. It is not completely clear how large an impact this amount of partial density scaling has on the overall results, although past dynamic studies (Itasca Consulting Group, Inc., 1996) have indicated that some partial density scaling is acceptable. It should be noted that the density scaling is applied to the smallest zones and masses in the model, in this case immediately around the drift.

4 NUMERICAL RESULTS

4.1 HEATED EMPLACEMENT DRIFT UNDER EARTHQUAKE SHEAR LOADING

Earthquake shear wave loadings were applied to the discrete element model such that the three underground emplacement drifts were subjected to peak ground accelerations ranging from 0.2 to 0.4g. Table 3-1 shows the different earthquake loading conditions for the three different discrete element models (DEM). As indicated in the table, for the heated drift scenario, all three levels of earthquake shear loading (i.e., 0.2, 0.3, and 0.4g) were simulated for Case B. A shear loading of 0.3g was applied to Case B1 to study the influence of vertical joint orientation on the dynamic response, since both Case A and B had the same joint patterns. For Case A, earthquake shear loadings of 0.2 and 0.4g were simulated. For the unheated drift scenario, both Cases B and B1 were subjected to earthquake shear loadings of 0.4g after excavation of the drifts. Each of the above simulations incorporates the dynamic response based on both single and repeated earthquake events. Once the first earthquake loading cycle was completed, there was a 5-s delay before a second earthquake loading of the same amplitude was applied to investigate the extent of cumulative joint slip or convergence around the central drift. Numerous monitoring points were established to measure roof displacements, relative shear displacements along joints, velocities, displacements, stresses, and accelerations at various locations around the drift as shown in figure 4-1.

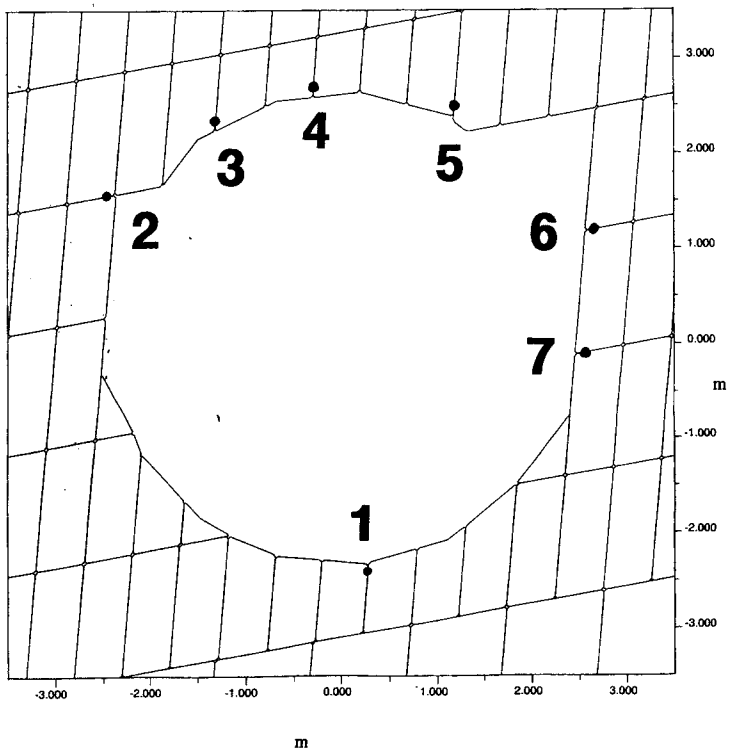

Figure 4-1. Location of monitoring points for relative shear displacements along joints. (Note: drift is at 100 yr thermal-mechanical loading state at which some rock fall occurred prior to dynamic loading).

The heated drift scenario involved subjecting the emplacement drift to a thermal load of 100 MTU/acre for a period of 100 yr as the starting point for the dynamic analysis. With regard to mechanical and thermal property input data for Case A, no yielding of the intact rock occurred during the TM loading stage. This TM loading stage produced maximum principal compressive stresses in the immediate roof and floor of approximately 75 MPa at the 100-yr thermal loading time. No additional rock mass yielding was experienced for Case A during either the repeated 0.2g or 0.4g earthquake loadings. The 0.4g earthquake loading results in a peak particle velocity of approximately 38 cm/s and maximum changes in dynamic shear stresses of approximately 2 MPa. Thus, the dynamic stresses generated in the rock mass are a small fraction of the combined *in situ*, excavation, and thermal stresses. For Case B, with a lower-end range of mechanical rock strength properties, yielding of the rock mass around the drift occurred during the 100-yr TM loading stage, and additional active yielding in shear took place during the higher 0.4g earthquake loading. In an actual underground environment, yielding of the rock as a result of earthquake loading may occur in the form of localized fracturing and spalling of rock, although this type of fracturing cannot presently be simulated in the model.

Figure 4-2 shows the additional vertical displacement in the roof in the central drift (i.e., thermal time = 100 yr) for Cases A and B under different levels of earthquake shear loading. Note that all displacements were zeroed out after the TM loading stage (i.e., upward expansion) so that the displacements plotted represent only those resulting from earthquake loading. Each case includes the effect of the two seismic loading cycles (the first earthquake loading was completed at t=30 s, followed by a 5-s delay before the second 30-s earthquake loading was initiated). For Case A in which the intact rock behaves elastically throughout the TM and seismic loading phases, no appreciable cumulative roof convergence is evident for either the 0.2g or 0.4g seismic loadings. However, for Case B in which the

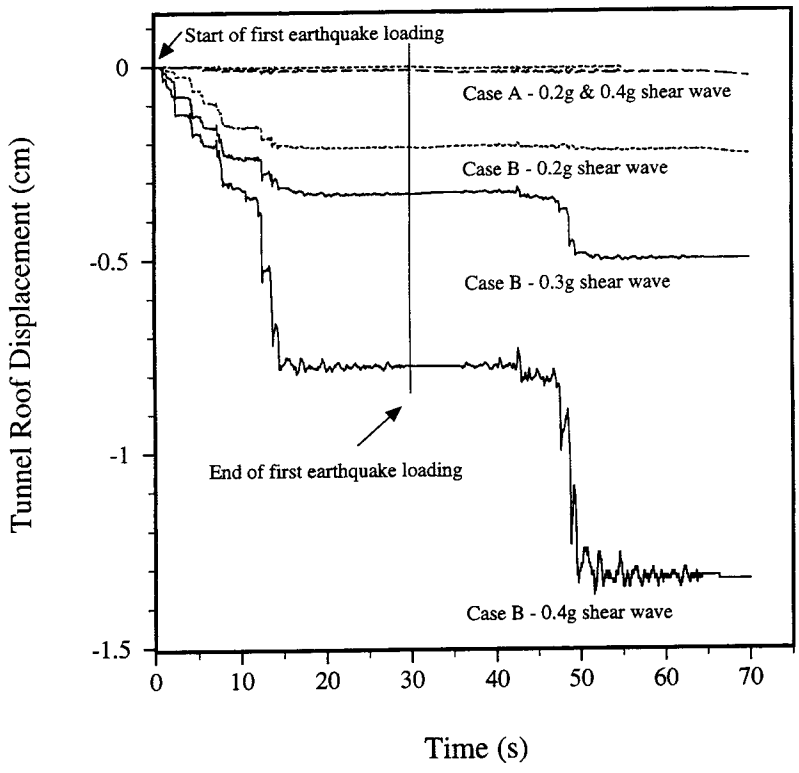

Figure 4-2. Additional vertical displacement at the mid-point of the roof in the central drift due to earthquake shear loading

rock is in a yielded state prior to seismic loading, definite cumulative deformations totalling 0.2, 0.35, and 0.8 cm take place after the first episode of earthquake shear loadings of 0.2, 0.3, and 0.4g, respectively. During the second earthquake shear loading episode for Case B, essentially no additional cumulative deformation occurs after repeating the 0.2g shear loading, while additional cumulative deformations of 0.15 and 0.5 cm occur after repeating the 0.3 and 0.4g shear loadings, respectively. It appears that, for the emplacement drift under a yielded state due to heating, there might be a threshold level (0.2g and below) where little or no cumulative roof deformation occurs with repeated episodes of earthquake loading. A possible explanation for the fact that the second earthquake loading results in less cumulative deformation than the first earthquake loading is given later in this section in the discussion on the change in stress states around the drift with dynamic loading. Results of a field investigation (Hsiung et al., 1992a and b) and an experimental study (Hsiung et al., 1997) have shown that cumulative deformation along joints and drift convergence occur in a stepwise manner with repeated seismic loadings. The model results show that this cumulative stepwise deformation of the drift occurs for some, but not all cases considered. As shown in figure 4-2, Case A shows essentially no deformation response for either cycle of dynamic loading.

Figures 4-3 and 4-4 show the additional relative shear displacements plotted with time for two of the seven monitoring points (see figure 4-1) that showed any measurable relative joint shear displacement as a result of seismic loading. Based on the UDEC sign convention, positive or negative relative joint shear is more or less immaterial, since it only indicates which direction one surface is sliding relative to the other. In figure 4-3, at monitoring Point 3 at the top of the tunnel, Case A again shows no relative slip along the subvertical joint intersecting the tunnel after earthquake shear loadings up to 0.4g peak ground accelerations. For Case B, figure 4-3 shows a definite cumulative relative joint shear displacement at Point 3 with both single and repeated earthquake shear loadings of 0.2, 0.3, and 0.4g, although the repeated shear loading at 0.2g results in essentially negligible accumulated relative shear displacement. Total accumulated relative shear displacements at Point 3 in the roof were 0.15, 0.32, and 0.67 cm for two repeated earthquake shear loadings having peak ground accelerations of 0.2, 0.3, and 0.4g, respectively. The increase in relative shear displacements between 0.3 and 0.4g events is much greater than that between 0.2 and 0.3g events. Figure 4-4 shows the relative joint slip along a subhorizontal joint intersecting the drift wall (Point 2). While there is some accumulated relative slip along these joints in the Case A model during the first episodes of earthquake shear loadings of 0.2 and 0.4g, there is little to none after the second episodes of earthquake loading. The results for the joint slip at Point 2 for Case B are similar in nature to those at Point 3.

Stress profiles along vertical and horizontal lines for Case B under TM and earthquake shear loadings (0.2g) are presented in figures 4-5 through 4-8. In general, as shown in figures 4-5 and 4-6, there is a small percentage increase in both the horizontal and vertical stress in the immediate roof after the earthquake loading. Further up into the roof, for a distance of about 30 m, there is a small percentage decrease in both the horizontal and vertical stresses. Almost all of these stress changes take place after the first earthquake loading. Similarly, as shown in figure 4-8, there is about a ten percent increase in the vertical stress immediately into the wall of the tunnel, followed by a similar decrease in vertical stress further into the wall after the earthquake shear loading. The horizontal stress in the wall of the tunnel (figure 4-7) does not appear to be affected much with the earthquake loading. The jagged nature of the stress profiles reflects the discontinuum (i.e., discrete block) representation of the system. The fact that there are stress increases in both the immediate wall and roof rock of the tunnel after the first episode of earthquake shear loading may be the reason why the accumulated deformations and joint slip are less for the second episode of dynamic loading than the first. For instance, the increase in horizontal stress within the roof after the first episode of dynamic loading will increase the compression along the near-vertical joint set, thus increasing their strength against slippage during the second episode of dynamic

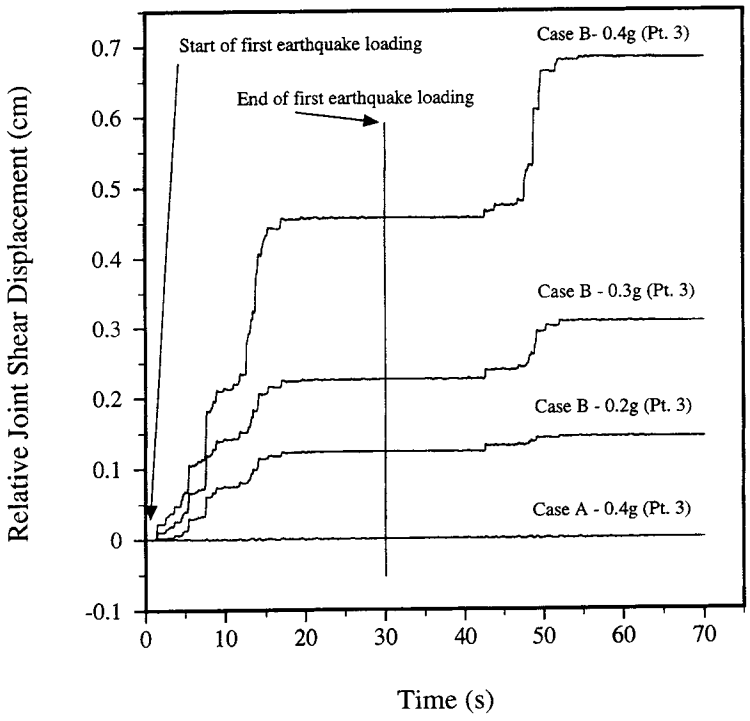

Figure 4-3. Additional relative joint shear displacement at Point 3 in the central drift (under heated condition) due to earthquake shear loading

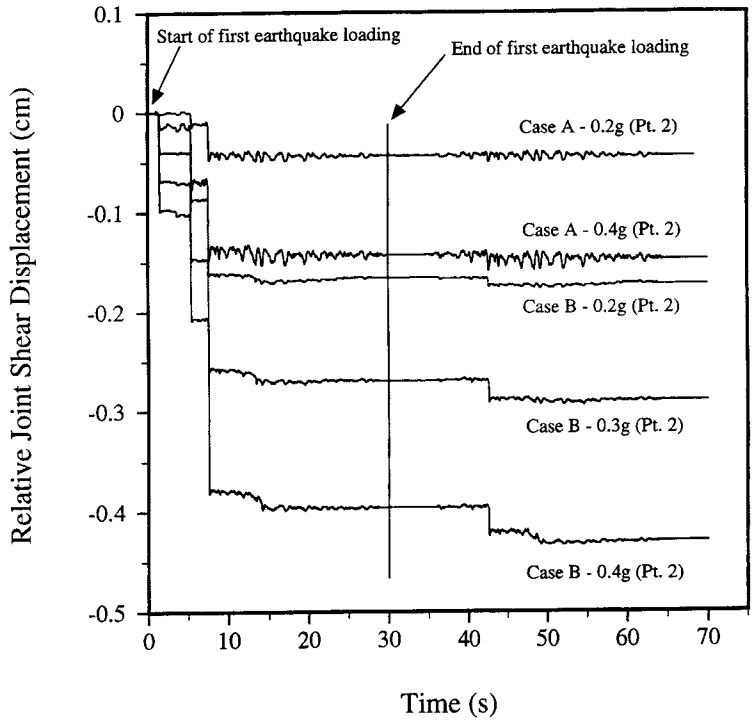

Figure 4-4. Additional relative joint shear displacement at Point 2 in the central drift (under heated condition) due to earthquake shear loading

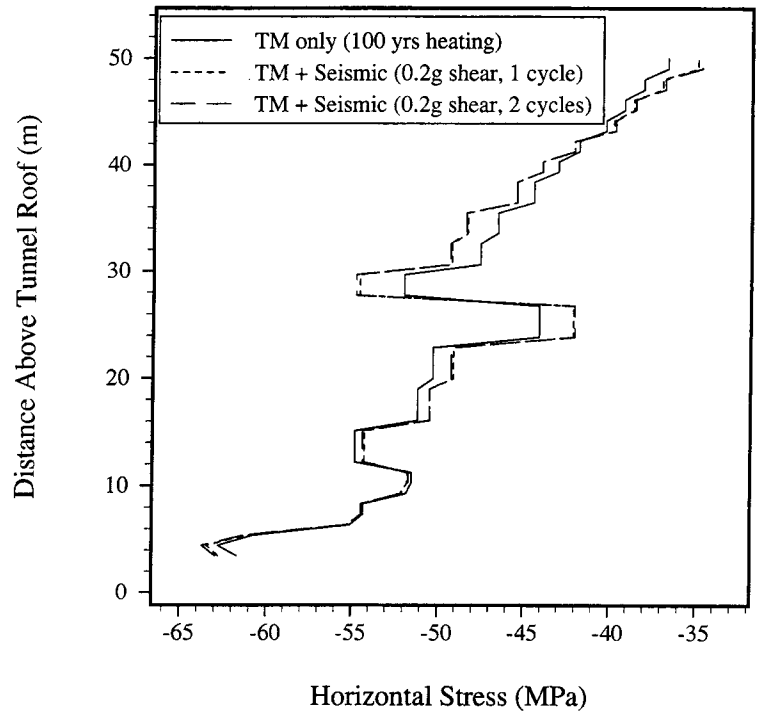

Figure 4-5. Horizontal stress profile in the drift roof for both thermal-mechanical and seismic loading (0.2g) for Case B

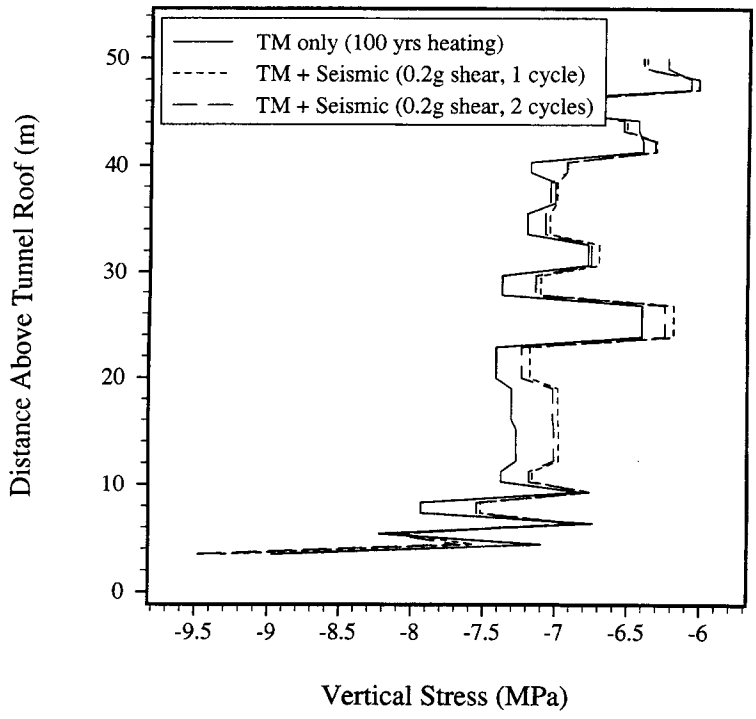

Figure 4-6. Vertical stress profile in the drift roof for both thermal-mechanical and seismic loading (0.2g) for Case B

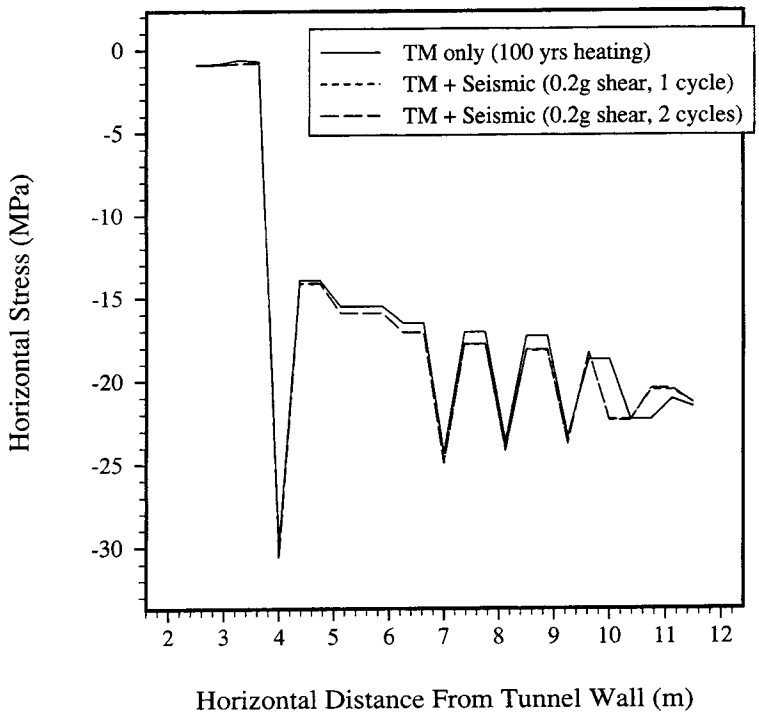

Figure 4-7. Horizontal stress profile in the drift wall for both thermal-mechanical and seismic loading (0.2g) for Case B

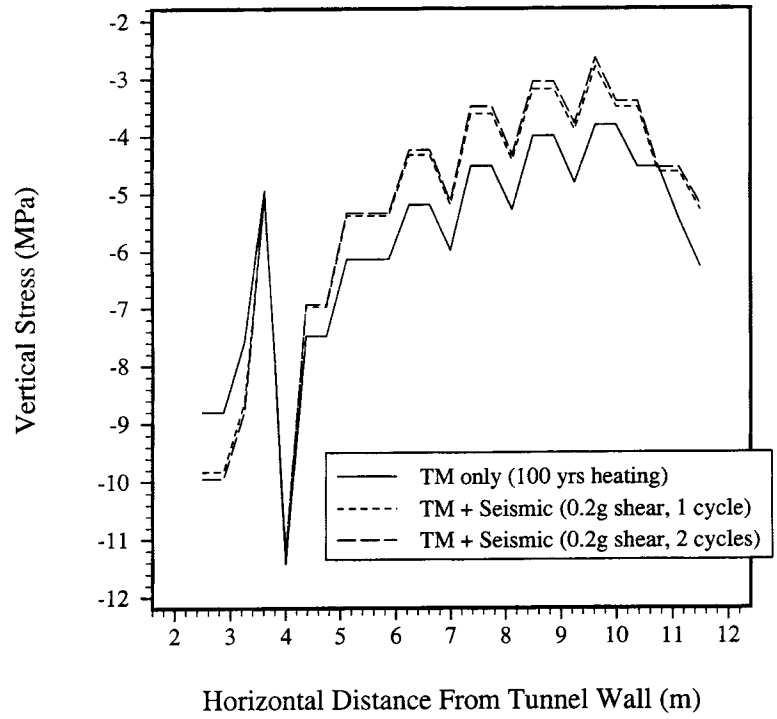

Figure 4-8. Vertical stress profile in the drift wall for both thermal-mechanical and seismic loading (0.2g) for Case B

loading. Likewise, the increase in vertical stress in the drift wall will have a similar effect on the near-horizontal joints. These stress increases in the immediate rock around the tunnel due to dynamic loading are much larger (up to 50 percent) for Case B under repeated earthquake loading of 0.4g, as shown in figures 4-9 through 4-12.

Figures 4-13 through 4-15 show the extent of Mohr-Coulomb plastic yielding around the heated drifts for Case B before earthquake loading and after repeated earthquake shear loadings of 0.3g and 0.4g peak acceleration, respectively. These three figures show that the outer lateral boundaries may have some influence on the yield zones around the outer two drifts because of the non-symmetrical jointing, which was partly the reason for extending the lateral dimension of the model from 1 to 3 drifts and analyzing only the central drift. The extent of the yield zone around the central drift for the Case B model is seen to increase with repeated earthquake loadings at both the 0.3g and 0.4g levels, as indicated by the increase in the extent of yield zones. Similarly, figures 4-16 and 4-17 show the extent of plastic yielding around the heated emplacement drifts for Case B1 both before earthquake loading, and after repeated 0.3g earthquake loadings, respectively. As mentioned earlier, Case B1 is identical to Case B except that instead of the subvertical joint orientation being 85° from the horizontal axis (measured counter-clockwise), it is lowered to 70°. Comparing figures 4-13 and 4-16 it can be seen that the extent of the yield zone is much less for Case B1 than for Case B, even though the material property and strength parameters are the same. As will be shown later, the lower subvertical joint orientation results in lower maximum principal stresses around the drift. Applying repeated earthquake shear loadings at 0.3g to Case B1 results in no additional plastic yielding around the drift (figure 4-17) as compared with that due to TM loading alone (figure 4-16). The repeated 0.3g dynamic loading, however, did result in a slight increase in plastic yielding for Case B (figure 4-14) over that due to TM loading alone (figure 4-13), as indicated by the increase in number of zones of past yielding. Recall that no rock yielding occurred for any of the earthquake shear loadings for Case A.

Maximum shear displacements along joints both before and after earthquake shear loading are provided in figures 4-18 through 4-24 for all three cases. For Case A, figures 4-18 and 4-19 show that essentially no additional shear displacement takes place after repeated earthquake shear loadings of 0.4g. For Case B, figures 4-20 through 4-22 show a gradual increase in both the magnitude and extent of joint shear displacements along the subhorizontal joints after TM loading (3.47 cm maximum), repeated 0.3g earthquake loadings (3.58 cm maximum), and repeated 0.4g earthquake loadings (6.26 cm maximum), respectively. This compares with only 1.5 cm maximum joint shear displacement for Case A. Finally, for Case B1, figures 4-23 and 4-24 show the joint shear displacements after TM loading (2.01 cm maximum) and repeated 0.3g earthquake loadings (2.12 cm maximum). Again both the extent and magnitude of joint shear displacements are less for Case B1 than for Case B for the same earthquake loading of 0.3g.

Maximum principal stress vectors (Note: compression negative) both before and after earthquake shear loading are provided in figures 4-25 through 4-31 for all three cases. Although the principal stress profiles appear similar before and after earthquake loading, the magnitudes of both the maximum compressive stress and maximum tensile stress increase after the dynamic loading. This is consistent with the discussion earlier regarding the horizontal and vertical stress profiles around the drift. Note that the initial TM stress state for Case B (figure 4-27) is quite a bit higher than that for Case B1 (figure 4-30), causing the larger extent of plastic yielding. For all case studies, some instability in the form of rockfall was experienced after the TM loading stage (e.g., figures 4-27 and 4-30), even though this same rock appeared stable after the excavation stage. No additional rockfall was experienced during any of the earthquake loading simulations, although increased yielding of intact rock was observed due to dynamic loading for some cases. This additional yielding might lead to rock fall if the code had the capability to simulate fracture or breakage of intact rock.

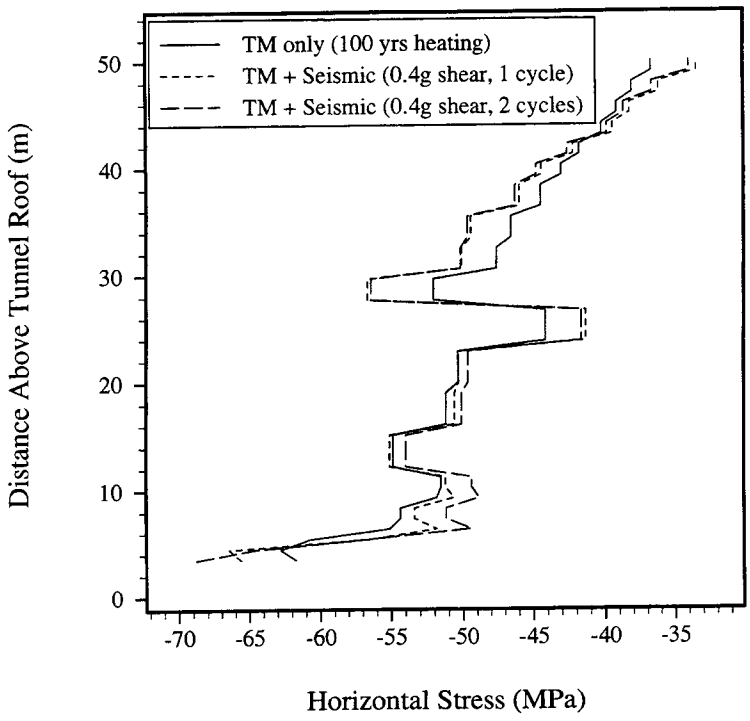

Figure 4-9. Horizontal stress profile in drift roof for both thermal-mechanical and seismic loading (0.4g) for Case B

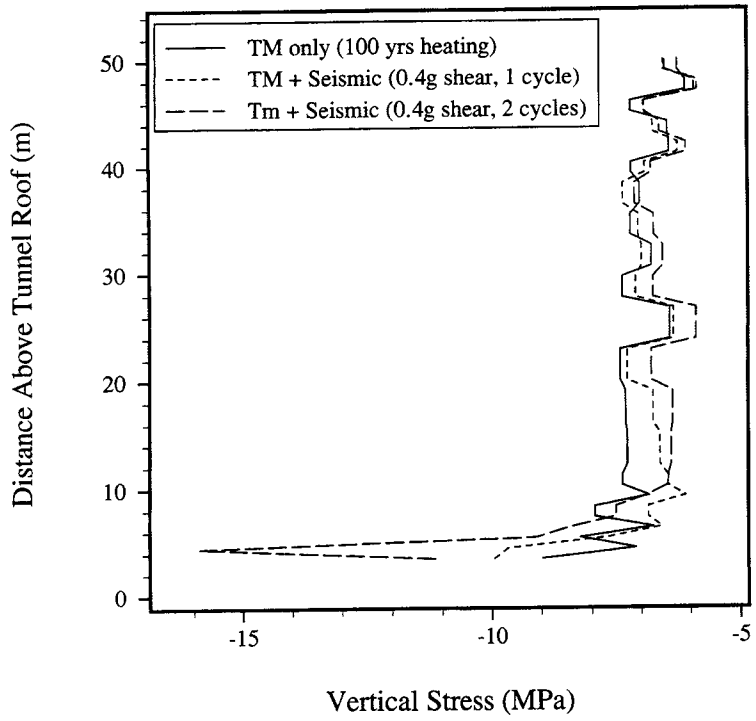

Figure 4-10. Vertical stress profile in drift roof for both thermal-mechanical and seismic loading (0.4g) for Case B

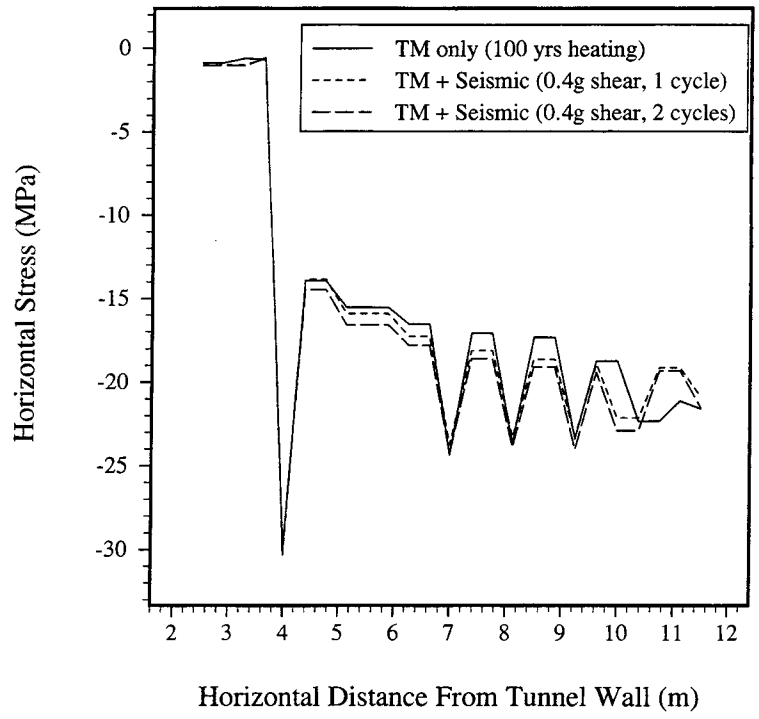

Figure 4-11. Horizontal stress profile in drift wall for both thermal-mechanical and seismic loading (0.4g) for Case B

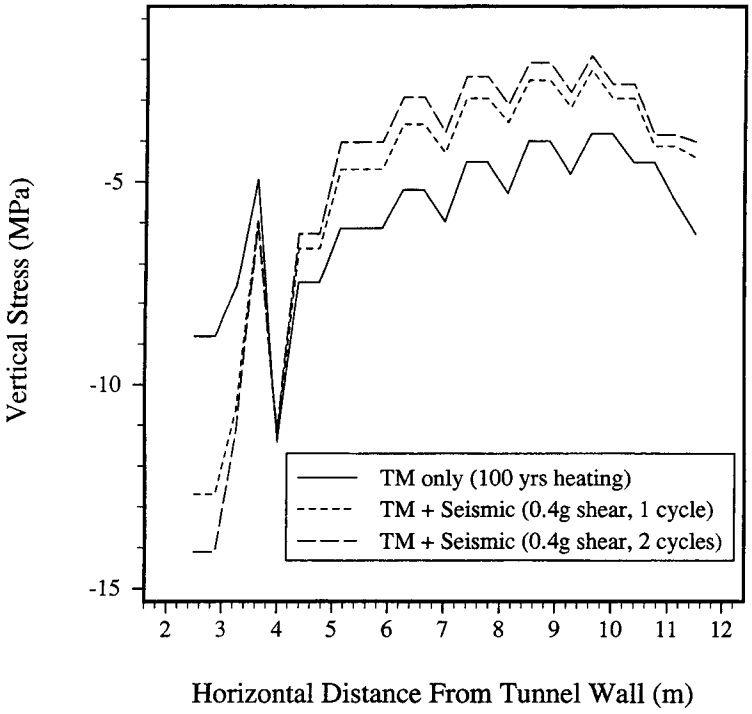

Figure 4-12. Vertical stress profile in drift wall for both thermal-mechanical and seismic loading (0.4g) for Case B

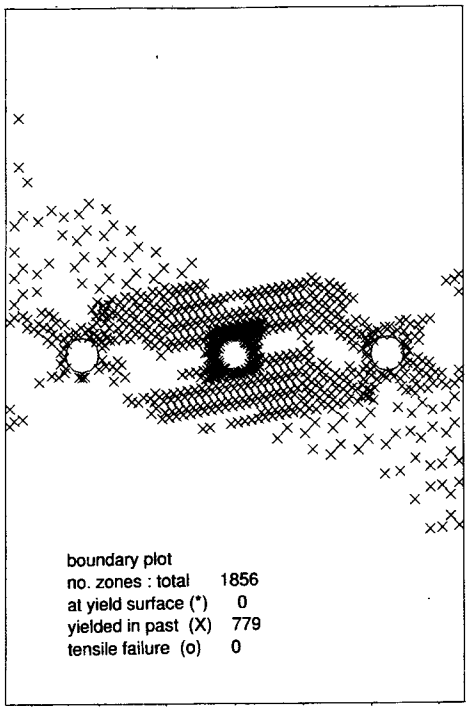

Figure 4-13. Extent of intact block yield zone after thermal-mechanical loading for Case B

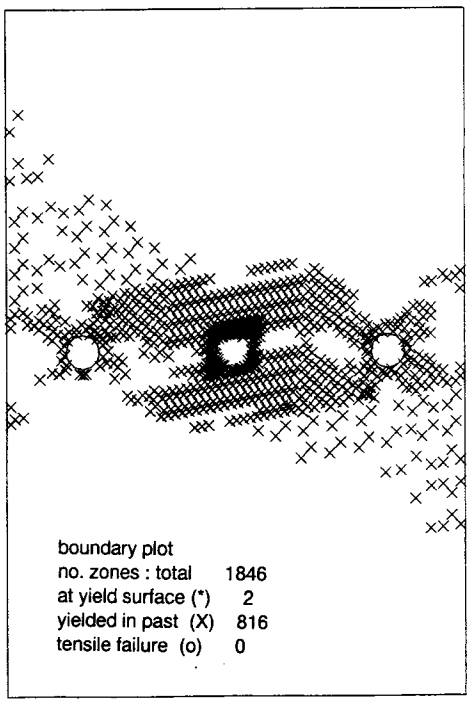

Figure 4-14. Extent of intact block yield zone after thermal-mechanical loading and earthquake shear loading (0.3g, two repetitions) for Case B. [Note: Total number of zones has decreased due to deletion of falling (yielded) blocks from 100 yr thermal-mechanical loading.]

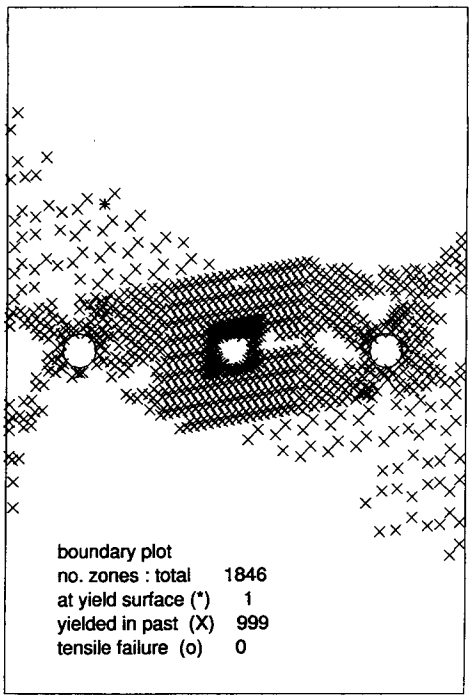

Figure 4-15. Extent of intact block yield zone after thermal-mechanical loading and earthquake shear loading (0.4g, two repetitions) for Case B

4.2 EXCAVATED (UNHEATED) DRIFT UNDER EARTHQUAKE SHEAR LOADING

To obtain an indication of whether an excavated but unheated drift is more susceptible to earthquake damage than a heated drift due to the lower state of stress, Cases B and B1 were subjected to 0.4g earthquake shear loadings immediately after the excavation phase. Figure 4-32 shows the additional downward vertical displacement of the roof after single and repeated earthquake loadings. Comparing with figure 4-2, it is seen that for Case B, the downward deflection of the roof is greater if the earthquake loading occurs after the thermal loading than before the thermal loading. Figures 4-33 through 4-36 show the principal stress vectors and joint shear displacements both after excavation (i.e., no thermal loading) as well as after earthquake loading of 0.4g. More specifically, while some rock appears to be marginally stable without rock support after excavation (figure 4-33), it is no longer stable after earthquake loading (figure 4-35). Comparing these two figures, it is seen that, again, both the maximum compressive stress (negative) and maximum tensile stress increase around the drift after the earthquake loading. However, in viewing the stress plots closely, one sees that the vertical component of stress in both the roof and floor appears to decrease. Examining the plots of joint shear displacement after excavation (figure 4-34) and earthquake shear loading (figure 4-36), it is seen that the maximum joint shear displacements are only on the order of a few millimeters rather than on the order of centimeters when taking into account the thermal loading as discussed in section 4.1. Also, without the thermal load and subsequent thermal expansion, the joint shear displacements are restricted to primarily the vertical joints even after earthquake loading, which was not the case in the discussion in section 4.1. Figures 4-37 through 4-40 show similar principal stress vector and joint shear displacement plots after excavation and after earthquake shear loading for Case B1. Again, as seen be these figures, reducing the orientation of the subvertical joints from 85° to 70° leads to results that are similar in nature to that for Case B.

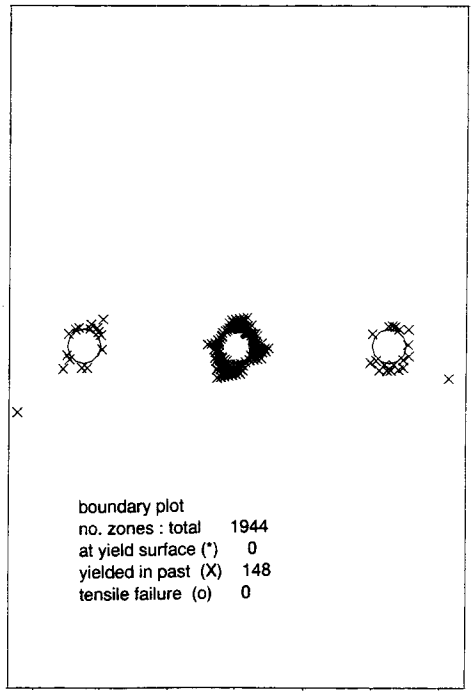

Figure 4-16. Extent of intact block yield zone after thermal-mechanical loading for Case B1

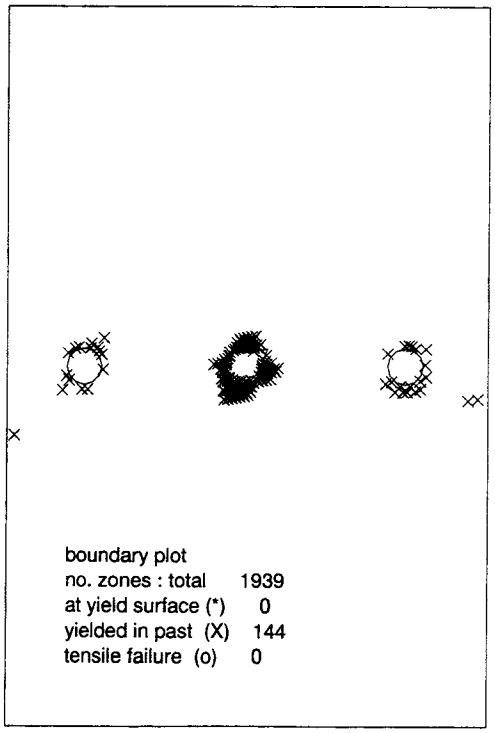

Figure 4-17. Extent of intact block yield zone after thermal-mechanical loading and earthquake shear loading (0.3g, two repetitions) for Case B1. [Note: Total number of zones and yielded zones smaller due to deletion of falling (yielded) blocks after 100 yr for loading.]

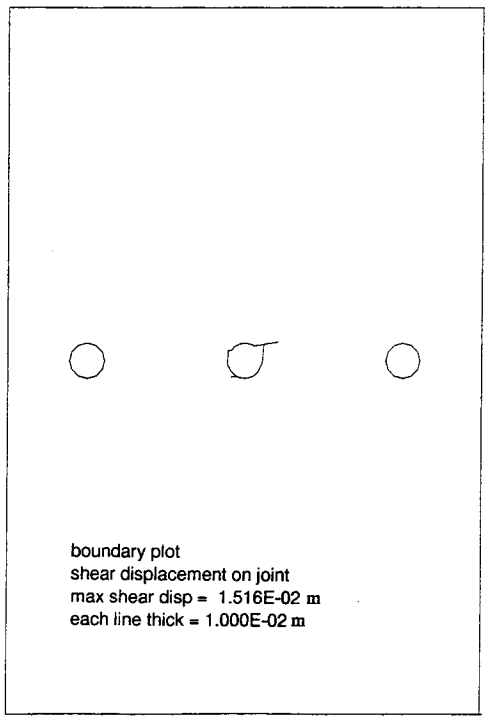

Figure 4-18. Shear displacement along joints after thermal-mechanical loading for Case A

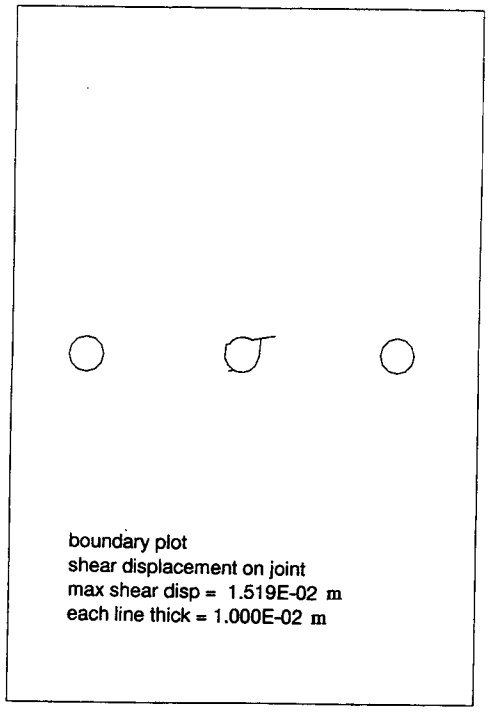

Figure 4-19. Shear displacements along joints after thermal-mechanical loading and earthquake shear loading (0.4g, two repetitions) for Case A

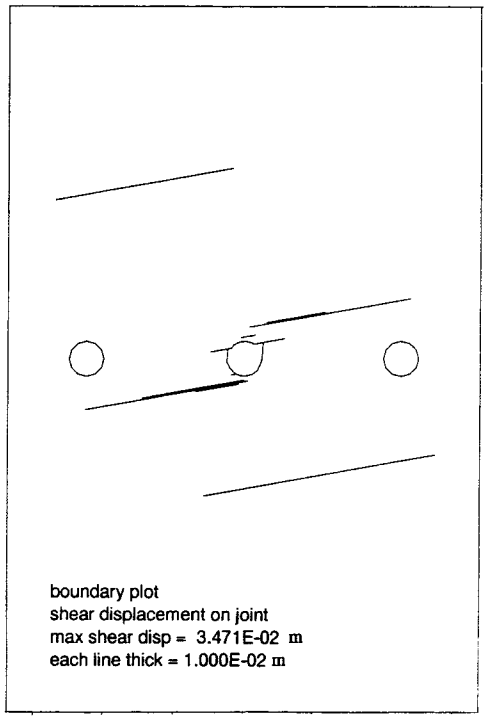

Figure 4-20. Shear displacements along joints after thermal-mechanical loading for Case B

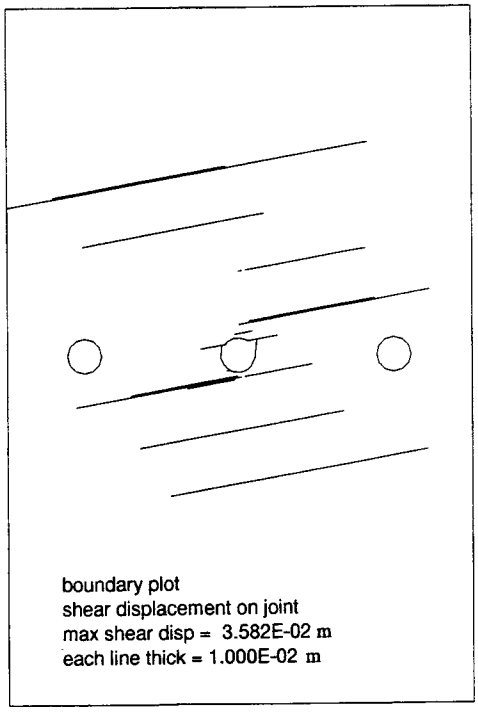

Figure 4-21. Shear displacements along joints after thermal-mechanical loading and earthquake shear loading (0.3g, two repetitions) for Case B

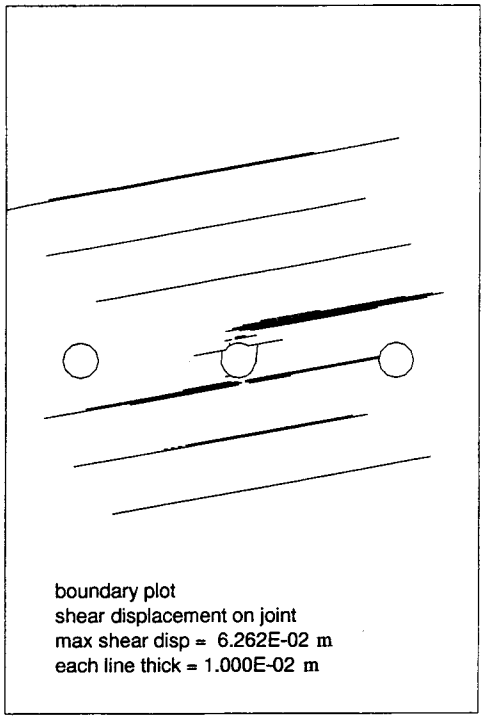

Figure 4-22. Shear displacements along joints after thermal-mechanical loading and earthquake shear loading (0.4g, two repetitions) for Case B

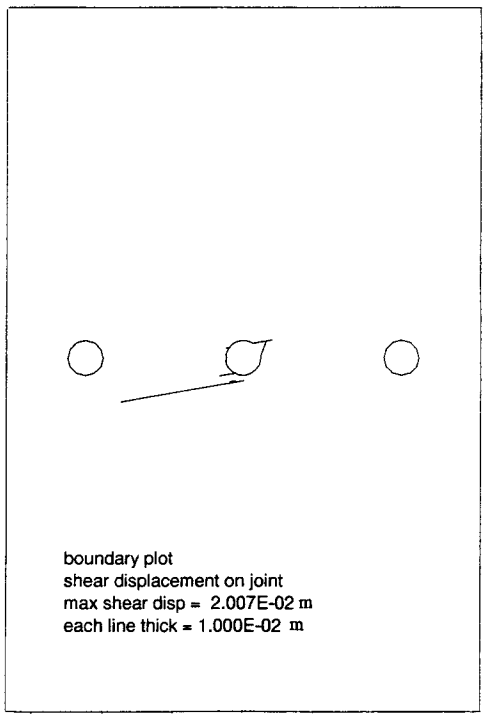

Figure 4-23. Shear displacements along joints after thermal-mechanical loading for Case B1

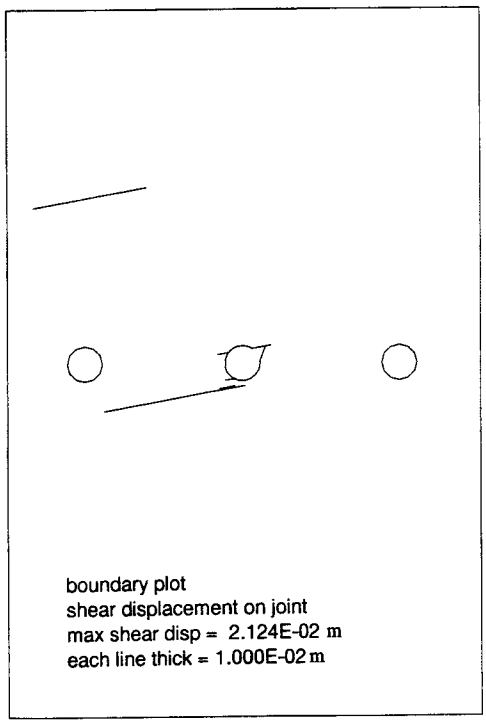

Figure 4-24. Shear displacements along joints after thermal-mechanical loading and earthquake shear loading (0.3 g, two repetitions) for Case B1

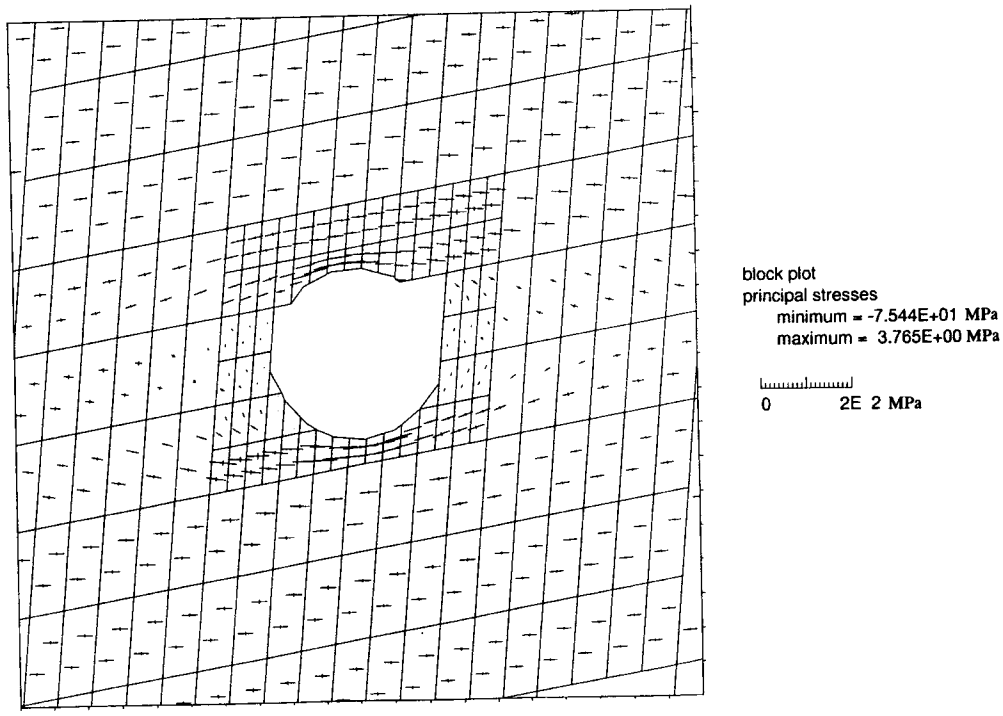

Figure 4-25. Principal stress vectors after thermal-mechanical loading for Case A

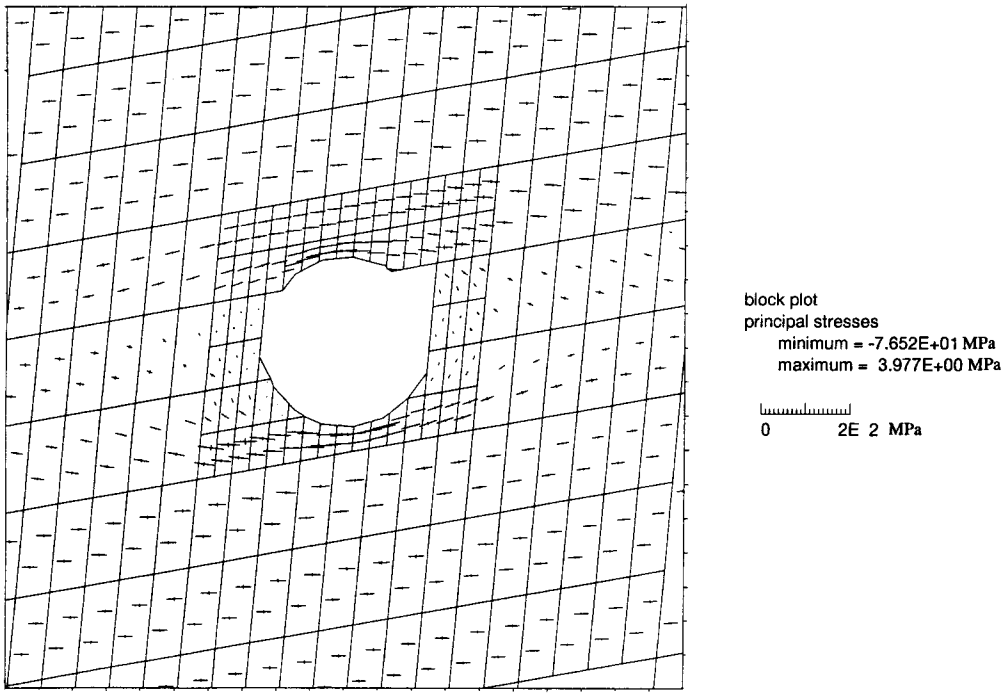

Figure 4-26. Principal stress vectors after thermal-mechanical and earthquake shear loading (0.4g, two repetitions) for Case A

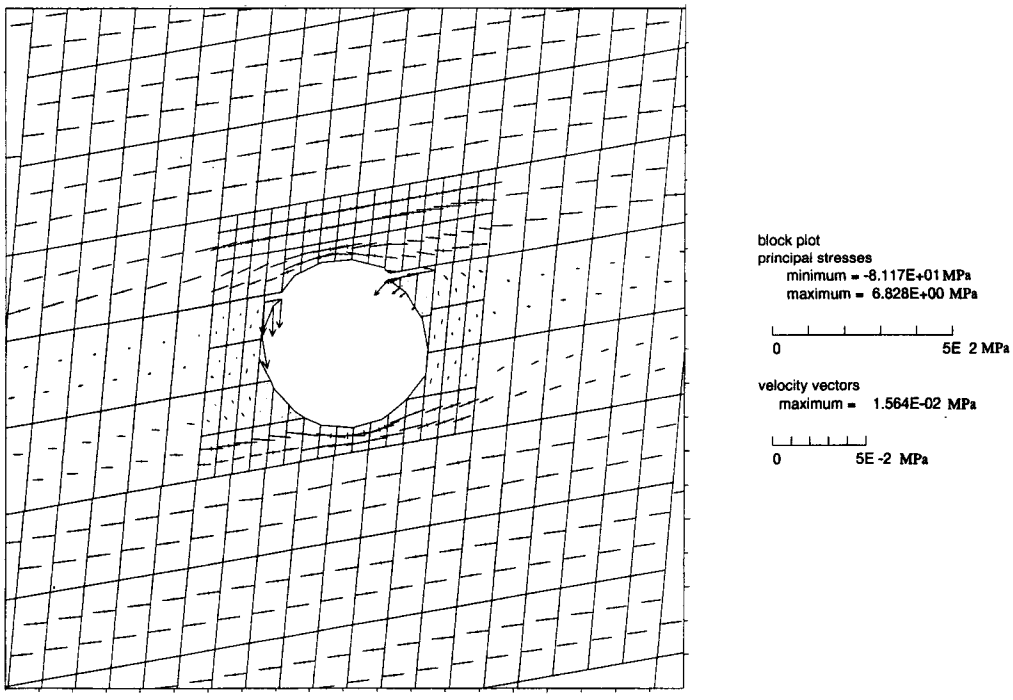

Figure 4-27. Principal stress and velocity vectors after thermal-mechanical loading for Case B

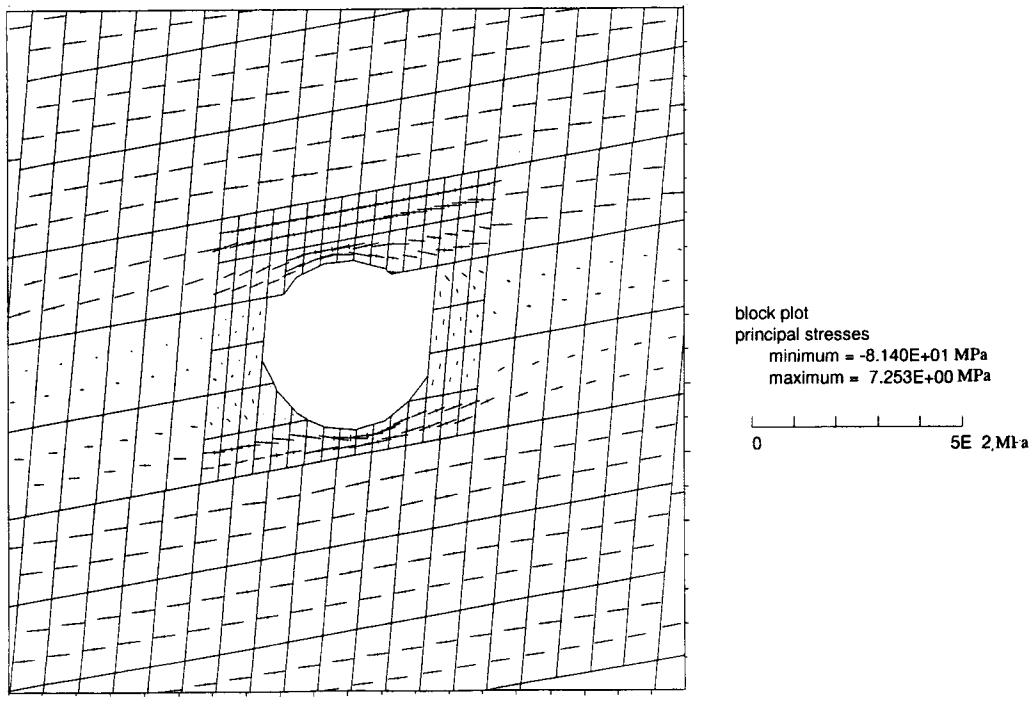

Figure 4-28. Principal stress vectors after TM loading and earthquake shear loading (0.3g, two repetitions) for Case B

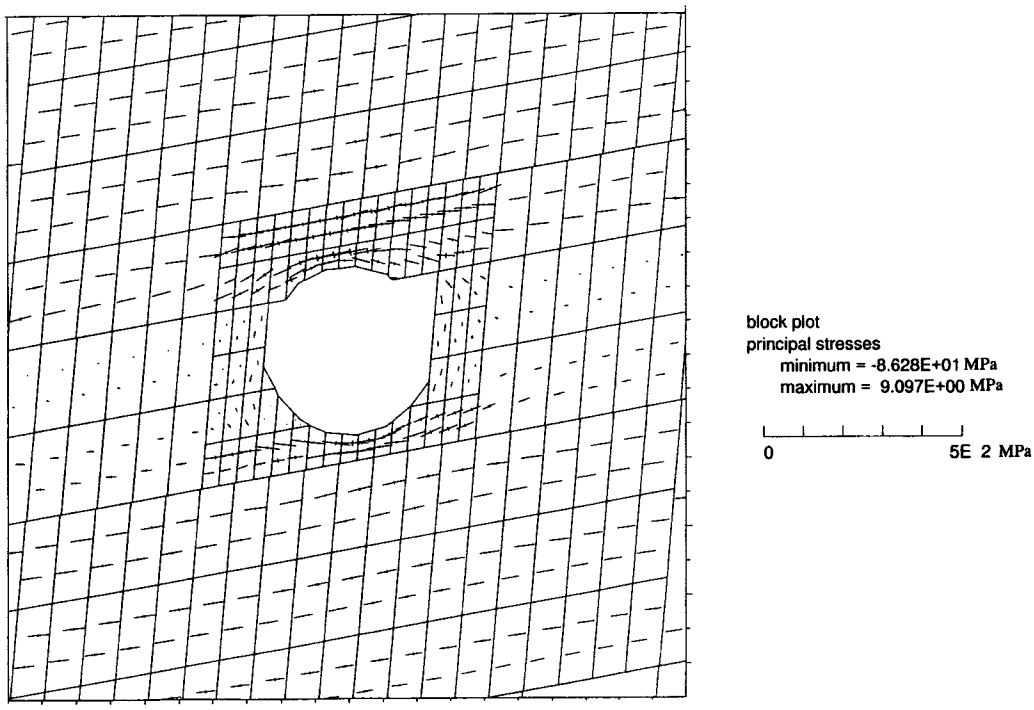

Figure 4-29. Principal stress vectors after TM loading and earthquake shear loading (0.4g, two repetitions) for Case B

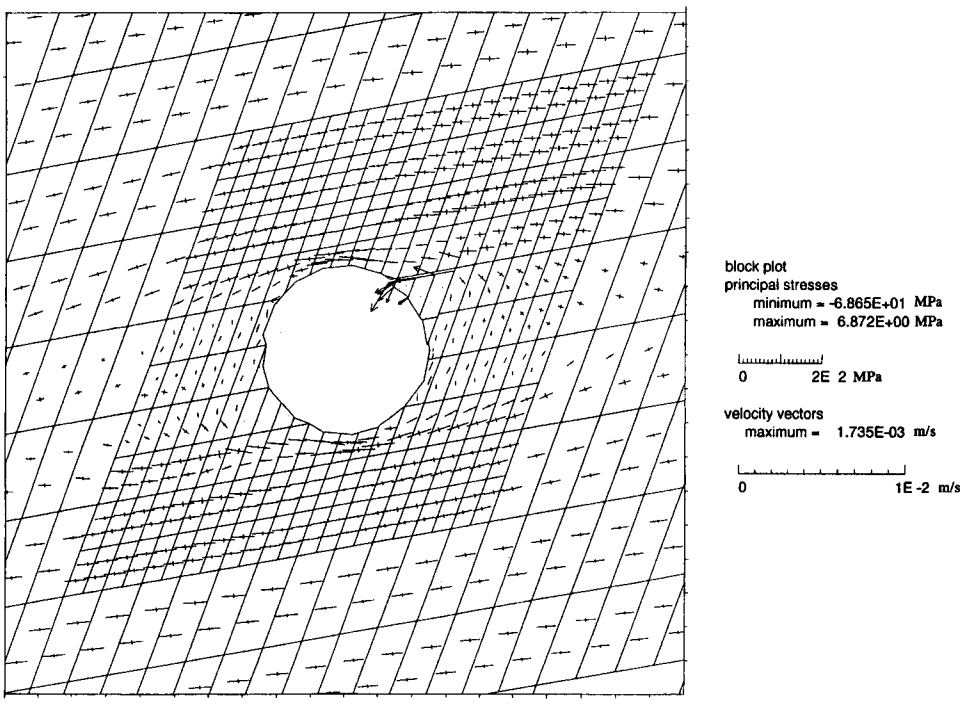

Figure 4-30. Principal stress vectors after thermal-mechanical loading for Case B1

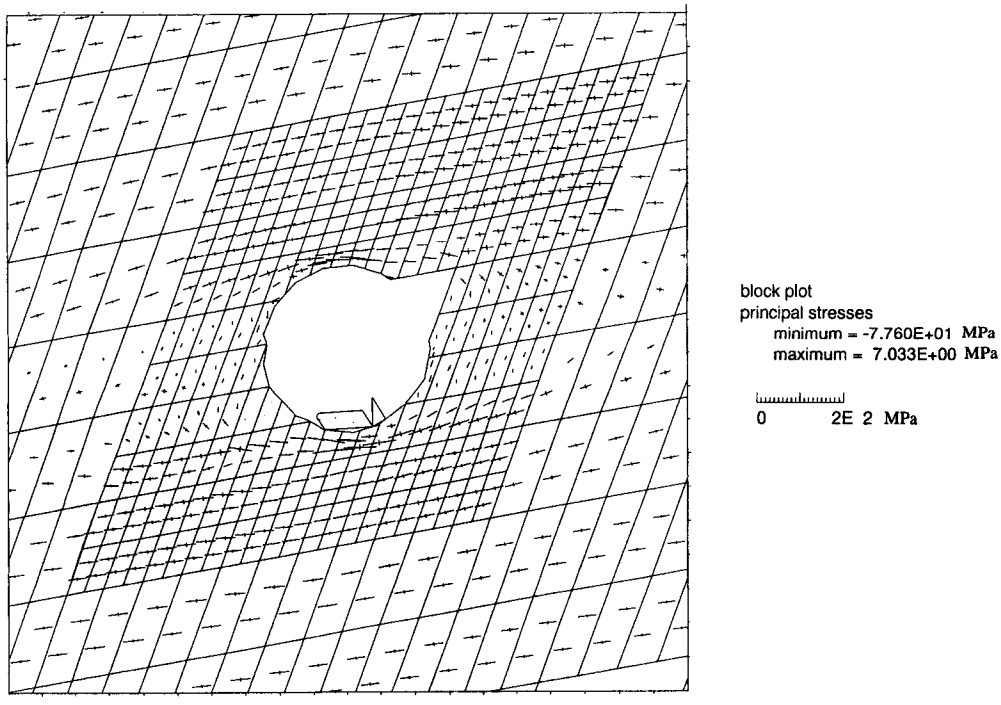

Figure 4-31. Principal stress vectors after thermal-mechanical loading and earthquake shear loading (0.3g, two repetitions) for Case B1

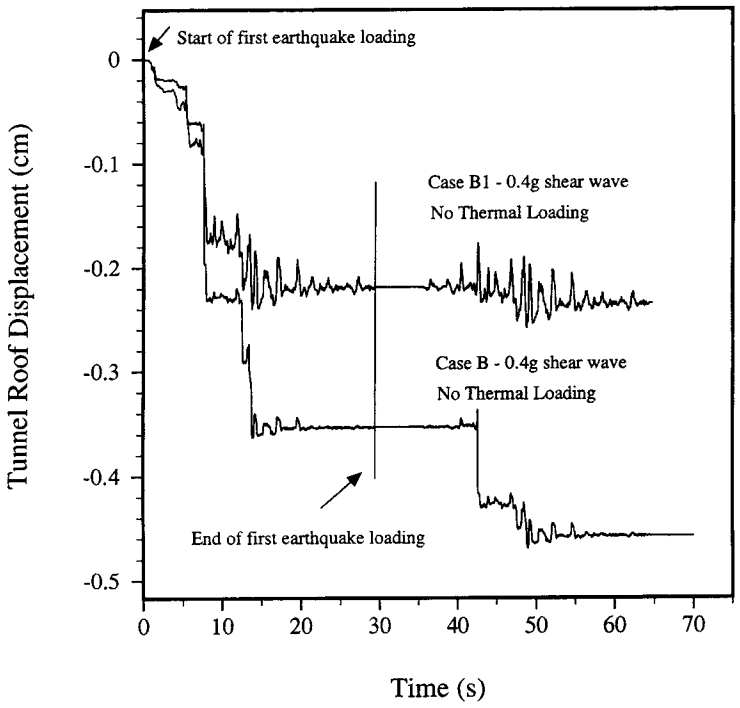

Figure 4-32. Additional vertical displacement of the drift roof (midpoint) with earthquake loading for a drift under no thermal loading

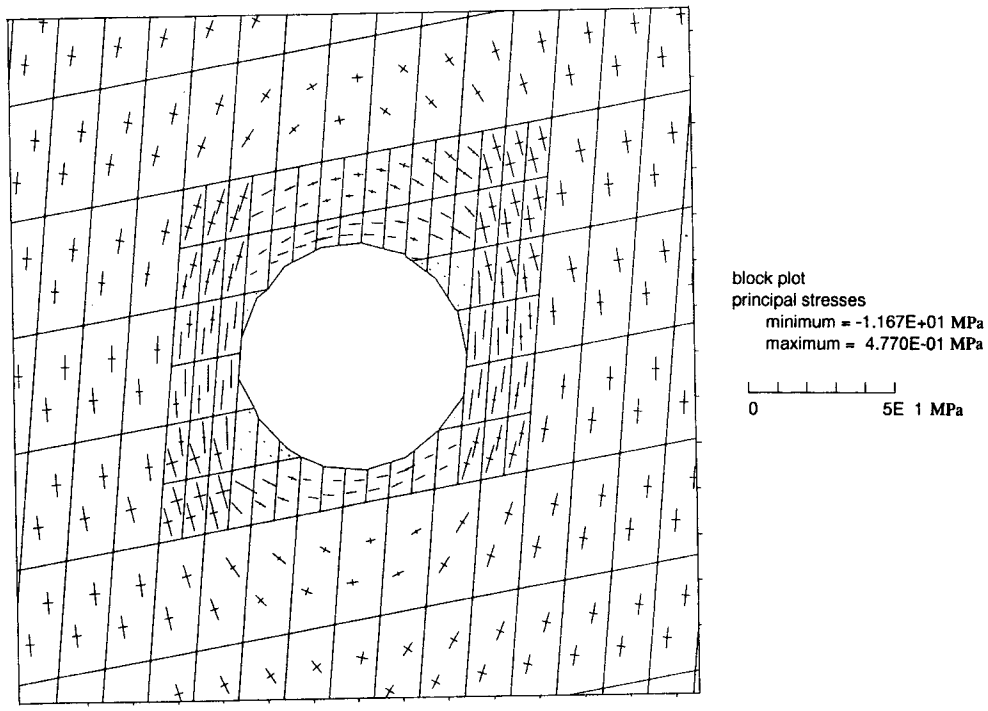

Figure 4-33. Principal stress vectors after excavation for Case B

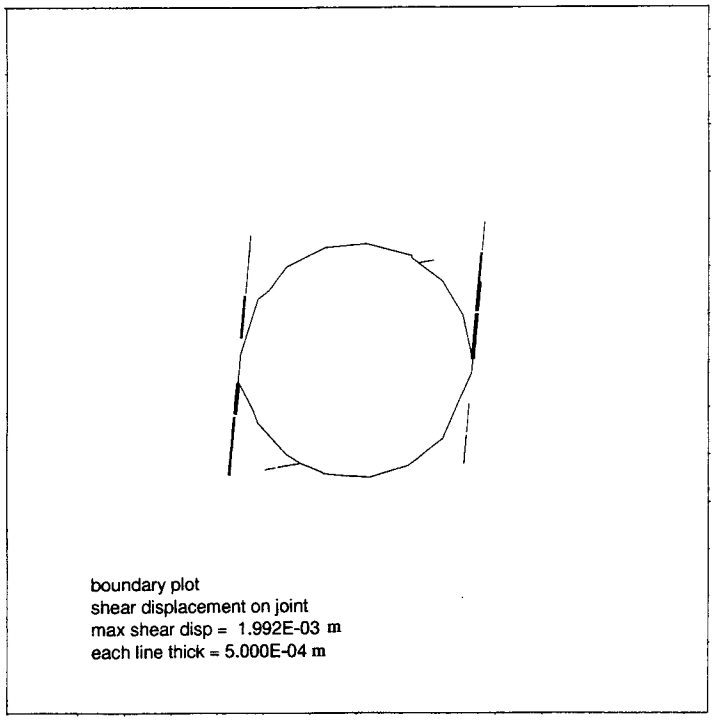

Figure 4-34. Joint shear displacements after excavation for Case B

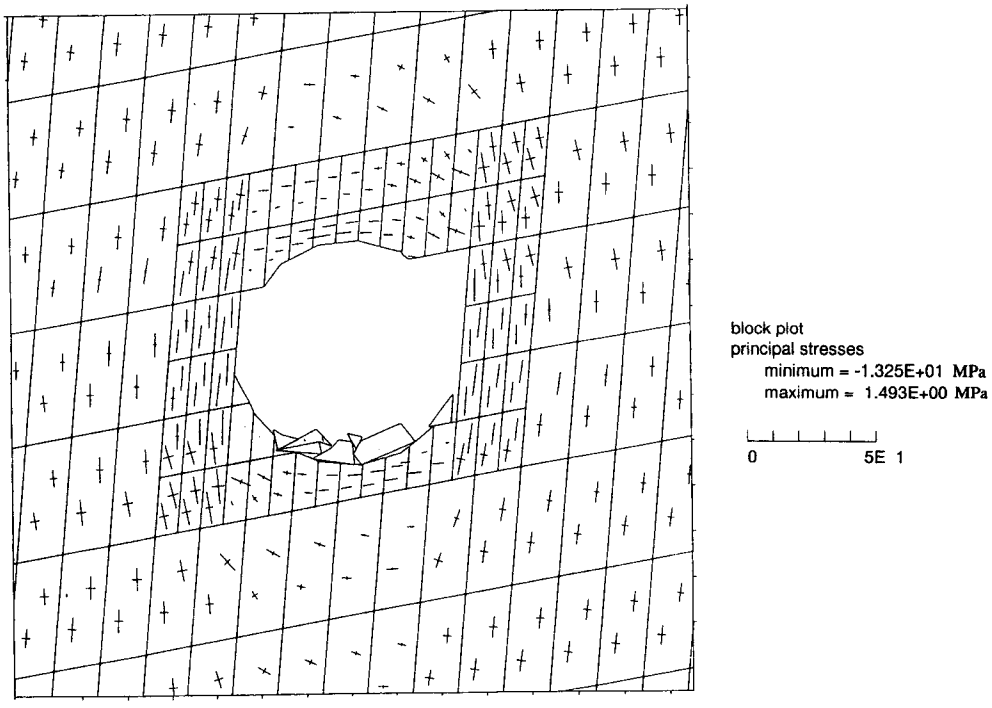

Figure 4-35. Principal stress vectors after earthquake shear loading of 0.4g (two repetitions, no thermal load) for Case B

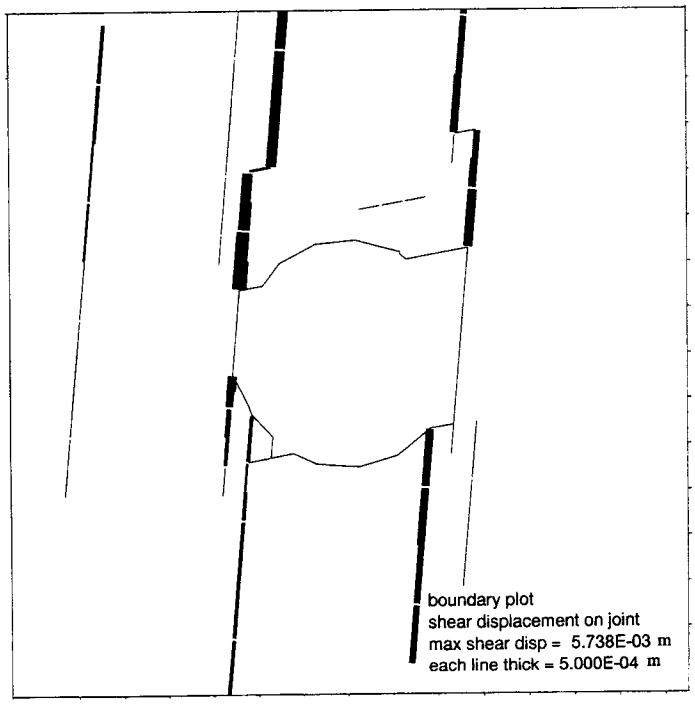

Figure 4-36. Joint shear displacements after earthquake shear loading of 0.4g (two repetitions, no thermal load) for Case B

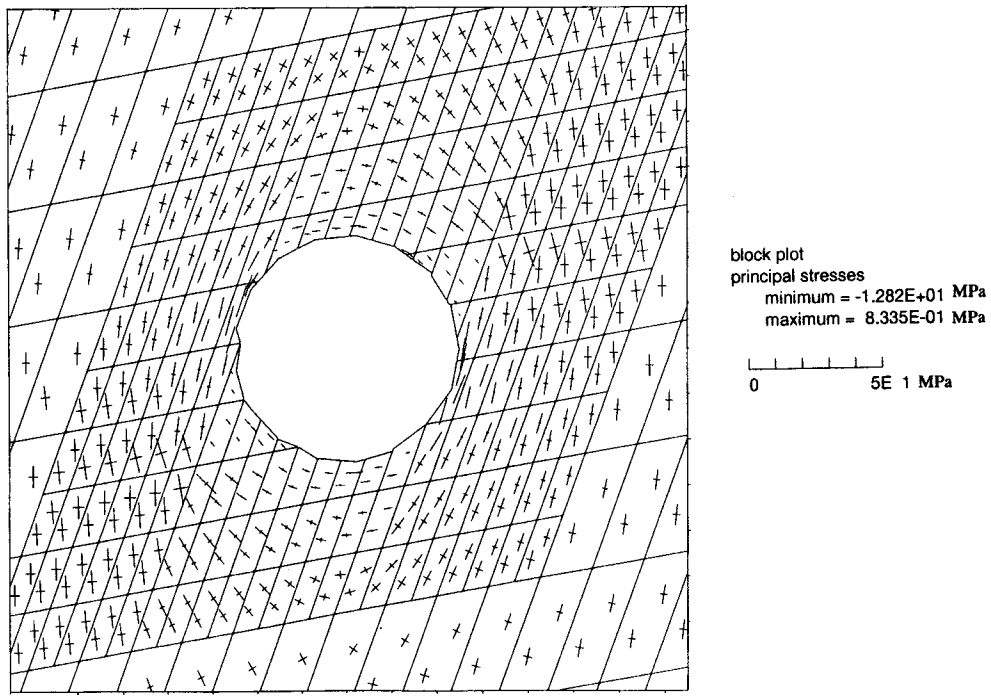

Figure 4-37. Principal stress vectors after excavation for Case B1

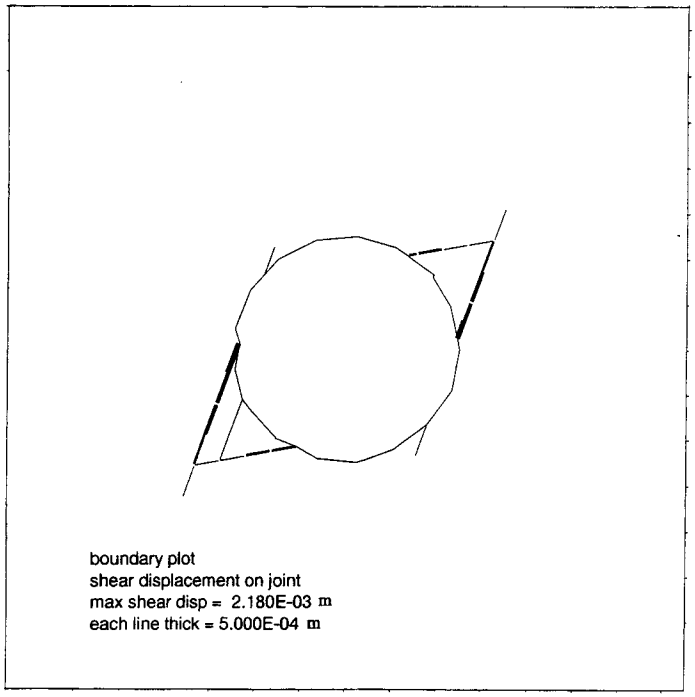

Figure 4-38. Joint shear displacements after excavation for Case B1

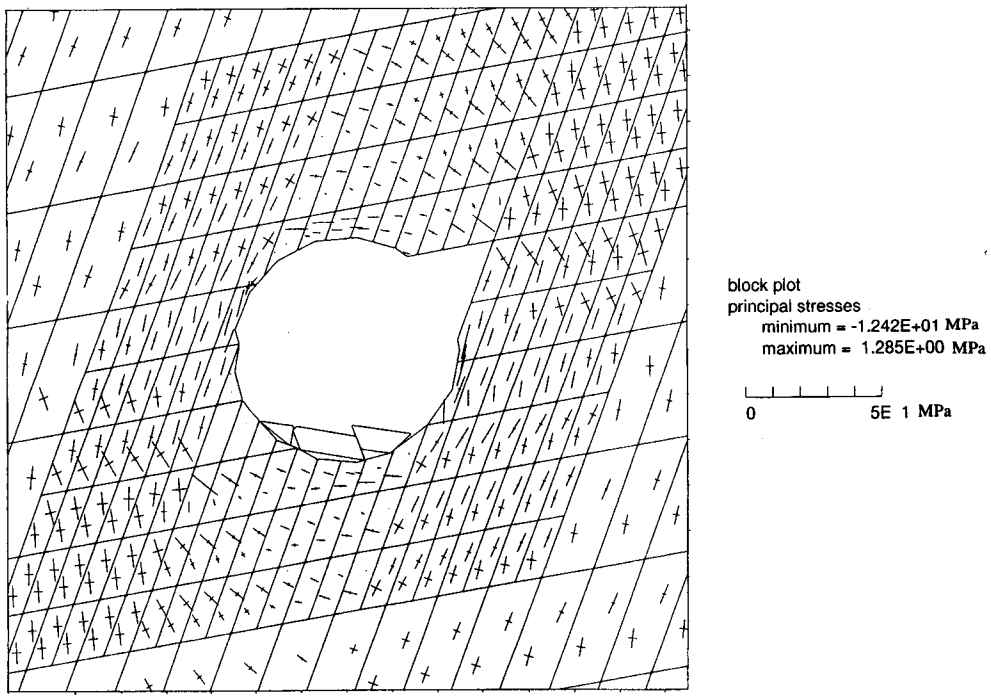

Figure 4-39. Principal stress vectors after earthquake shear loading of 0.4g (two repetitions, no thermal loading) for Case B1

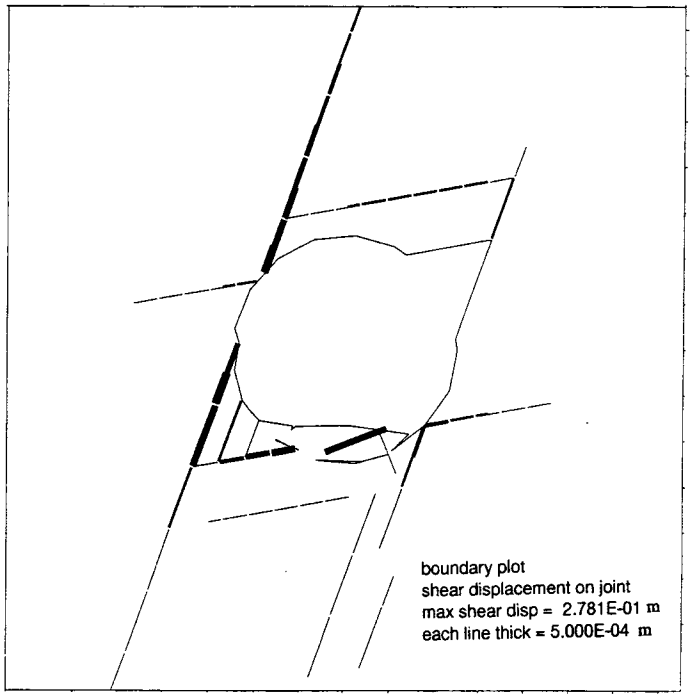

Figure 4-40. Joint shear displacements after earthquake shear loading of 0.4g (two, repetitions, no thermal loading) for Case B1

5 SUMMARY AND CONCLUSIONS

A distinct element analysis was conducted to investigate the stability of waste emplacement drifts at the proposed YM nuclear waste repository site under seismic loading. Earthquake loadings having peak underground accelerations ranging from 0.2 to 0.4g and durations of approximately 30 s were analyzed, including both single and repeated events. The drifts were assumed to be in a heated, unsupported, and unbackfilled state, although two cases were analyzed assuming no thermal loading. Cumulative deformation along joints intersecting the drift and increased drift convergence were experienced with repeated dynamic loading for cases B and B1, where the rock mass around the drift was in a weakened or yielded state after the thermal loading and prior to the dynamic loading. No cumulative drift convergence was experienced for Case A with repeated dynamic loading. Also, shearing along joints intersecting the drift in Case A occurred only along the sub-horizontal joints, and only during the first episode of dynamic loading. The maximum total roof deflection after two repeated episodes of earthquake loadings was approximately 1.8 cm for the range of loadings and cases considered. Maximum joint shear displacements (occurring along the subhorizontal joint set) were approximately 6.3 cm for the range of earthquake loadings and cases considered. Although some additional rock yielding around the drift took place for some of the cases during dynamic loading, no additional rock instability was evident relative to the thermal loading stage. However, without the thermal load, marginally stable rock after excavation became unstable after the earthquake loading. In general, the incremental displacements and stress changes resulting from the second episode of earthquake loading were less than those resulting from the first episode of earthquake loading. This may be due somewhat to the observation that immediately around the drift the maximum and/or minimum principal stresses increased after the first episode of earthquake loading. For instance, the increase in horizontal stress within the immediate roof after the first episode of dynamic loading resulted in increased normal compression along the near-vertical joints. This increase in joint normal stress would make such joints less susceptible to slip during the second dynamic event. Likewise, the increase in vertical stress in the drift wall after the first dynamic event increases the compressive normal stress on the sub-horizontal joints, lessening their tendency to slip with a second dynamic event. It was observed that, for the set of thermal and mechanical material properties considered, a steeper vertical joint orientation (i.e., 85° versus 70° measured from the horizontal) resulted in more damage from both TM and earthquake loading in terms of the amount of rock yielding, maximum joint shear displacements, and drift convergence.

A number of limitations in the Phase II UDEC modeling should be noted. Some of these limitations required certain assumptions to be made in order to complete the modeling tasks. These limitations/assumptions are listed below with recommendations for possible future improvements.

(i) During the thermal-mechanical loading stage, the decaying heat flux was applied directly to the circular perimeter of the drifts. This was necessary since UDEC does not simulate radiant heat transfer from a heat-generating body or mass within a cavity (i.e., drift). Also, since the analysis was for an unbackfilled drift, the only plausible approach to input the thermal loading was as a heat flux to the tunnel wall. In the unsupported drift scenario this creates problems as certain discrete blocks around the tunnel perimeter in which the heat flux is being applied separate and begin to collapse into the tunnel, since the thermal logic assumes a continuum. The approach taken was not to allow too much separation to occur in these unstable blocks during the 100 yr TM run to allow the heat flux to continue to be applied through the blocks. Certain thermal tolerances were increased so that even though there was some separation between blocks, the calculational scheme assumed they were in thermal contact. Enough mechanical time cycling was done so that the remainder of the rock mass was in TM equilibrium aside from a few unstable blocks around the tunnel. Although this approach appeared to work, it slowed the TM run times considerably, making it impractical to look at the influence of seismic effects long into the cool down period of the repository. Possible recommendations for future

improvements might be to either include cavity radiation behavior within UDEC, or alternatively run the thermal analysis separately for the continuum, and modify the code to periodically read updated nodal temperatures for the corresponding thermal-mechanical discontinuum analysis.

(ii) Although the intact rock was modeled as a Mohr-Coulomb elastic-plastic material with tension cut-off to identify zones of yielding around the tunnel in shear and tension, it was necessary for the Phase II dynamic analysis to increase the tensile rock strength around the tunnel to avoid any failure in tension. When a portion of a discrete block (i.e., one finite-difference zone) fails in tension, UDEC assumes that particular zone or gridpoint essentially becomes unsupported. For the unsupported drift analysis, if any such mid-nodes or gridpoints of a block edge along the perimeter of the drift fail in tension, that portion of the block begins to grossly elongate downwards while the remainder of the block is still supported within the rock. This scheme will work if support (e.g., a concrete liner) is modeled, but creates problems when no support is modeled. One recommendation for future analyses would be to modify the code to create a tensile fracture through such a block, in which a portion of that block could collapse and redistribute the loads as necessary.

(iii) UDEC has a fairly limited set of material models compared to other commercial codes (i.e., ABAQUS and DYNA3D). Non-linear material models in Version 3.0 of UDEC essentially consist of either elastic/plastic Mohr-Coulomb (used in this study) or Drucker-Prager failure criteria, although the built in "FISH" programming language allows for some flexibility in terms of a user-defined constitutive model. It is possible that such models may not adequately simulate the brittle failure nature of rock, especially that of the densely welded tuff at the proposed repository horizon. Based on field measurements from field-scale heater tests, it may be prudent in future studies to incorporate better material models into subsequent analyses. In particular, if monitoring of field-scale thermomechanical experiments shows brittle fracturing within the intact rock, that type of brittle fracturing phenomenon should be incorporated into failure of intact discrete element blocks within the model.

(iv) For this dynamic study, it was necessary to apply partial mass density scaling to small discrete element blocks within the model to increase the dynamic timestep incorporating both stiffness and mass proportional damping. The effect of this partial mass density scaling was assumed to be negligible; however, it should be verified for any future analysis. This is especially true since the artificial density scaling is applied to the small blocks near the tunnel. Subsequent dynamic analyses should also investigate ways to speed up the dynamic analysis either increasing the dynamic timestep or other means.

(v) In order to model realistic joint spacings around the tunnel while at the same time keeping the dynamic computational run times reasonable, various transition zones in blocks sizes were necessary, even for the submodel approach adopted for the dynamic study. It is expected that such transition zones from finer to coarser blocks creates some stiffness contrasts that may artificially induce slip on such interfaces during the TM and dynamic simulations. In viewing the results, this effect is thought to be negligible, but may warrant further investigation.

The cumulative effect of repeated seismic loading observed for Cases B and B1 in this study appears consistent with the findings of earlier field and laboratory studies (Hsiung et al., 1992a and b; Hsiung et al., 1997). Case A was more or less insensitive to both single and repeated dynamic loadings, and appears to contradict laboratory and field studies. The reason for this should be more fully investigated. It should be noted that these findings are based only on a small set of parametric studies, because dynamic time step requirements, computation times, as well as programmatic constraints, prohibited a more

exhaustive analysis. Also, because of computational requirements, the spacing of joints considered in this study might be somewhat larger than that existing underground, most likely making the analysis less conservative from that standpoint. Future underground mappings of joints should verify this, and be factored into the interpretation of the results. Finally, calibration of the excavation and thermal-mechanical stresses and deformations obtained from the modeling study with those obtained from ongoing and future DOE field-scale heater tests should be conducted to gain further confidence in the dynamic modeling predictions.

6 REFERENCES

Ahola, M.P., R. Chen, H. Karimi, S.M. Hsiung, and A.H. Chowdhury. 1996. *A Parametric Study of Drift Stability in Jointed Rock Mass Phase I: Discrete Element Thermal-Mechanical Analyses of Unbackfilled Drifts*. CNWRA 96-009. San Antonio, TX: Center for Nuclear Waste Regulatory Analyses.

Althaus, E., A. Friz-Töpfer, Ch. Lempp, and O. Natau. 1994. Effects of water on strength and failure model of coarse-grained granites at 300 °C. *Rock Mechanics and Rock Engineering*. 27(1): 1–21.

Barr, D.L., T.C. Moyer, W.L. Singleton, A.L. Albin, R.C. Lung, S.C. Beason, A.C. Lee, and G.L.W. Eaton. 1996. *Geology of the North Ramp - Station 4+00 to 28+00, Exploratory Studies Facility, Yucca Mountain Project*. Yucca Mountain, Nevada, Bureau of Reclamation and U.S. Geological Survey, Prepared in cooperation with the Nevada Field Office, U.S. Department of Energy (DE-A108-92NV10874).

Brown, E.T. and J.A. Hudson. 1974. Fatigue failure characteristics of some models of jointed rock. *Earthquake Engineering and Structural Dynamics*. 2: 379–386.

Carter, N.L. 1975. High-temperature flow of rocks. *Reviews of Geophysics and Space Physics*. 13(3): 344–349.

Carter, N.L. 1976. Steady state flow of rocks. *Reviews of Geophysics and Space Physics*. 14(3): 301–360.

Civilian Radioactive Waste Management System Management and Operating Contractor (CRWMS M&O). 1996. *Mined Geologic Disposal System Advanced Conceptual Design Report*. Volume II. B00000000-01717-5705-00027 Rev 00. Las Vegas, NV: Civilian Radioactive Waste Management System.

Civilian Radioactive Waste Management System Management and Operating Contractor (CRWMS M&O). 1994a. *Initial Summary Report for Repository/Waste Package Advanced Conceptual Design*. B00000000-01717-5705-00015 Rev 00. Las Vegas, NV: Civilian Radioactive Waste Management System.

Civilian Radioactive Waste Management System Management and Operating Contractor (CRWMS M&O). 1994b. *Seismic Design Inputs for the Exploratory Studies facility of Yucca Mountain*. B00000000-01717-5705-00001 Rev 02. Las Vegas, NV: Civilian Radioactive Waste Management System.

de Marsily, G. 1987. An overview of coupled processes with emphasis on geohydrology. *Coupled Processes Associated with Nuclear Waste Repositories*. C.F. Tsang, ed. San Diego, CA: Academic Press: 27–37.

Dowding, C.H. 1985. Earthquake Response of Caverns: Empirical Correlations and Numerical Modeling. *Proceedings 1985 Rapid Excavation and Tunneling Conference*. C.D. Mann and M.N. Kelley, eds. New York, NY: American Institute of Mining, Metallurgical, and Petroleum Engineers.

Dowding, C.H., and A. Rozen. 1978. Damage to Rock Tunnels from Earthquake Shaking. *ASCE Journal of Geotechnical Engineering Division* 104: 229–247.

Ghosh, A., S.M. Hsiung, G.I. Ofoegbu, and A.H. Chowdhury. 1994. *Evaluation of Computer Codes for Compliance Determination Phase II.* CNWRA 94-001. San Antonio, TX: Center for Nuclear Waste Regulatory Analyses.

Hoek, E., and E.T. Brown. 1980. *Underground Excavation in Rock.* London, UK: The Institution of Mining and Metallurgy.

Hoffman, R.B. 1994. *SEISM 1.1 Test Analysis.* CNWRA 94-014. San Antonio, TX: Center for Nuclear Waste Regulatory Analyses.

Hsiung, S.M., W. Blake, A.H. Chowdhury, and T.J. Williams. 1992a. Effects of mining-induced seismic events on a deep underground mine. *PAGEOPH* 139(3/4): 741–762.

Hsiung, S.M., A.H. Chowdhury, W. Blake, M.P. Ahola, A. Ghosh. 1992b. *Field Site Investigation: Effect of Mine Seismicity on a Jointed Rock Mass.* CNWRA 92-012. San Antonio, TX: Center for Nuclear Waste Regulatory Analyses.

Hsiung, S.M., A.H. Chowdhury, A. Ghosh, and D.J. Fox. 1997. Laboratory investigation of seismic effects on underground excavations in jointed rock mass. *International Journal of Rock Mechanics and Mining Sciences* 34: 3-4, Paper No. 101.

Itasca Consulting Group, Inc. 1996. *UDEC - Universal Distinct Element Code.* Version 3.0. Volume I: User's Manual. Minneapolis, MN: Itasca Consulting Group, Inc.

Jaeger, J.C., and N.G.W. Cook. 1979. *Fundamentals of Rock Mechanics.* 3rd Edition. London, UK: Chapman and Hall, Ltd.

Kana, D.D., B.H.G. Brady, B.W. Vanzant, and P.K. Nair. 1991. *Critical Assessment of Seismic and Geomechanics Literature Related to a High-Level Nuclear Waste Underground Repository.* NUREG/CR-5440. Washington, DC: Nuclear Regulatory Commission.

Kana, D.D., D.J. Fox, S.M. Hsiung, and A.H. Chowdhury. 1995. *An Experimental Scale-Model Study of Seismic Response of an Underground Opening in Jointed Rock Mass.* CNWRA 95-012. San Antonio, TX: Center for Nuclear Waste Regulatory Analyses.

Kemeny, J., and N.G.W. Cook. 1990. Rock mechanics and crustal stress. *Demonstration of Risk-Based Approach to High-Level Waste Repository Evaluation.* R.K. McGuire, ed. EPRI NP-7057. Golden, CO: Risk Engineering Inc.: 5-1 to 5-20.

Klavetter, E.A., and R.R. Peters. 1986. *Estimation of Hydrologic Properties of an Unsaturated Fractured Rock Mass.* SAND84-2642. Albuquerque, NM: Sandia National Laboratories.

Lee, C.F., K.K. Tsui, and H.W. Asmis. 1982. Rock mechanics design of an underground CANDU nuclear power plant. *Proceedings from ISRM Symposium on Rock Mechanics: Caverns and Pressure Shafts* 2: 971–977. Ed. W. Wittke. Rotterdam, Netherlands: A.A. Balkama.

Lin, W., and W.D. Daily. 1989. Laboratory study of fracture healing in Topopah Spring tuff — implications for near field hydrology. *Nuclear Waste Isolation in Unsaturated Zone Focus '89 Proceedings.* La Grange Park, IL: American Nuclear Society: 443–449.

Manteufel, R.D., M.P. Ahola, D.R. Turner, and A.H. Chowdhury. 1993. *A Literature Review of Coupled Thermal-Hydrologic-Mechanical-Chemical Processes Pertinent to the Proposed High-Level Nuclear Waste Repository at Yucca Mountain*. NUREG/CR-6021. Washington, DC: Nuclear Regulatory Commission.

Martin III, R.J. 1972. Time-dependent crack growth in quartz and its application to the creep of rocks. *Journal of Geophysical Research* 77(8).

Nataraja, M.S., and T. Brandshaug. 1992. *Staff Technical Position on Geologic Repository Operations Area Underground Facility Design — Thermal Loads*. NUREG-1466. Washington, DC: Nuclear Regulatory Commission.

Nimick, F.B., and J.R. Connolly. 1991. *Calculation of Heat Capacities for Tuffaceous Units from the Unsaturated Zone at Yucca Mountain, Nevada*. SAND 88-3050. Albuquerque, NM: Sandia National Laboratories.

Nuclear Regulatory Commission. 1996. *Disposal of High-Level Radioactive Wastes in Geologic Repositories*. Title 10, Energy, Part 60 (10 CFR Part 60). Washington, DC: U.S. Government Printing Office.

Price, R.H., J.R. Connolly, and K. Keil. 1987. *Petrologic and Mechanical Properties of Outcrop Samples of the Welded, Devitrified Topopah Spring Member of the Paintbrush Tuff*. SAND86-1131. Albuquerque, NM: Sandia National Laboratories.

TRW Environmental Safety Systems, Inc. 1994. *Initial Summary Report for Repository/Waste Package Advanced Conceptual design*. Prepared for the U.S. Department of Energy. Document No. B00000000-01717-5705-00015, Volume I, Revision 00. Las Vegas, NV: TRW Environmental Safety Systems, Inc.

Tsang, C.F. 1987. Introduction to coupled processes. *Coupled Processes Associated with Nuclear Waste Repositories*. C.F. Tsang, ed. San Diego, CA: Academic Press: 1–6.

U.S. Department of Energy. 1988. *Site Characterization Plan: Yucca Mountain Site, Nevada Research and Development Area*. DOE/RW-0199. Washington, DC: U.S. Department of Energy.

U.S. Department of Energy. 1995. *Topical Report: Seismic Design Methodology for a Geologic Repository at Yucca Mountain*. YMP/TR-003-NP. Las Vegas, NV: U.S. Department of Energy.

Wang, J.S.Y., D.C. Mangold, R.K. Spencer, and C.F. Tsang. 1983. *Thermal Impact of Waste Emplacement and Surface Cooling Associated with Geologic Disposal of Nuclear Waste*. NUREG/CR-2910. Washington, DC: Nuclear Regulatory Commission.

Wilder, D.G. 1996. *Near-Field and Altered-Zone Environment Report. Volume II*. UCRL-LR-124998. Livermore, CA: University of California, Lawrence Livermore National Laboratory.